Knot probabilities and scaling exponents of ring polymer chains: effects of topology and excluded volume

UEHARA, Erica

Department of Physics, Ochanomizu University

Contents

1 Introduction

Human beings use various polymers such as foods, fibers and rubbers. This kind of materials had come from only nature for centuries. In fact, human beings believed that we could not produce polymers which are called organic compounds. Chemists synthesized polymers in the 19th century while they did not know what they created. In the 20th century, they realized that they had been making huge molecules of which the molecular masses are over 10^4 g/mol. We now produce and utilize a large amount of artificial polymers. For instance, we industrially synthesize Bakelite, polyvinyl chloride, nylon and polyethylene terephthalate.

In general, a synthesized polymer has branches in its C-C backbone. Many types of polymer architectures arise from branches: star-branched, comb, ladder and randomly-branched. It have been difficult to control random branching during polymerization, however, chemists succeed in purifying a dilute solution of ring polystyrenes, where the purity of ring polystyrenes is over 96% [1].

The solution of ring polymers of high purity is produced experimentally at present, however, it includes industrial interests. It is expected that the nature of ring polymers is different from that of linear polymers. Micelle comprising ring polymers is more thermostable than that of linear polymers. The viscosity of the solution of ring polymers will be smaller since ring polymers do not have ends and get less entanglement than linear polymers or branched polymers. In future, we will design a polymer with both its chemical identity and topological architecture.

A ring polymer has topological isomers: physicists and mathematicians addressed that each ring polymer may be knotted ring polymer as a topological isomer [9, 10]. It was proven rigorously that every self-avoiding walk on lattice is knotted if it is very long [15, 16]. Krasnow is the first person who saw a knotted ring polymer in the 1980s. He knotted circular DNA with type II topoisomerases and take the pictures of the knotted DNA by an electron microscope [2]. In the 1990s, Rybenkov and Show independently studied the knot probability of DNA in a solvent. They showed that the probability of being non-trivial knots depends on the concentration of counter ions in the solvent [3, 4]. Moreover, due to developments in experimental techniques, knotted ring polymers and such polymers with more complex topology than ring polymers are effectively synthesized [11, 12, 13, 14].

The knot probability of ring polymers have been studied also through simulations: In 1970s, Vologodskii et al. estimated the knot probability for random polygons (RP) with the maximum number of vertices N=150 [17]. Michels et al. showed that the knot probability of the trivial knot with N vertices decreases exponentially [18]. Due to improvement of methods for knot detection [7, 19], knot probabilities of non-trivial knots were evaluated for off-lattice RP or self-avoiding random polygons (SAP) with larger N [20, 21, 22, 23] and on-lattice random polygons [24, 25, 26, 27]. Knot probabilities for SAP consisting of cylinders were studied with different radius of cylinders and different number of vertices N up to 150 [28] or 1000 [29].

Topological effects is predicted to increase the mean-square radius of gyration of knotted ring polymers [32, 33, 34]. It was studied through simulation [37, 38, 39, 40] and can be measured in experiments. However, it is difficult to evaluate the exact scaling exponent of knotted ring polymers or random polygons.

The purpose of this thesis is to characterize the nature of knotted ring polymers through simulation. We generated RP and SAP consisting of cylindrical segments by Monte-Carlo method [5], detected their knot type [8, 9] and estimated the knot probabilities of RP and SAP. We introduced a new formula to express the knot probability. Our formula fitted well the knot probabilities of various types of knots. Moreover, it has less number of parameters than that of the previous one.

The contents of this thesis are as follows. Chapter 2 is provided for the illustration of the numerical method we employed. In Chapter 3, we show that knot probabilities of prime and composite knots are well expressed by our new formation. We find that characteristic lengths of knotting are almost the same for different types of knots and coefficients of the knot probability decrease as the radius of cylinders grows for all types of knots but 3_1 knot. In Chapter 4, we evaluate the mean-square radius of gyration of knotted random polygons.

1.1 Ideal and Self-avoiding walks

Flexibility mechanism and the persistence length

Consider a polyethylene molecule as a simple example for a polymer chain. The distance between carbon atoms in the backbone of the molecule is 1.54Å of which fluctuations are typically 0.05Å. The tetrahedral angle, the angle between successive C-C bonds, is about 68 degree. The distance and the tetrahedral angle are almost fixed; they do not contribute to the polymer flexibility.

The polymer flexibility is caused by the variation of torsion angles which neighboring 4 atoms define. They define the plane through the first 3 atoms C_1, C_2, and C_3, and that through the last 3 atoms C_2, C_3, and C_4. The torsion angle is the angle between these planes. We call the angle which corresponds to the lowest conformation energy the trans state of the torsion angle. Conformation energy has other minima; the second minima are called gauche-plus and gauche-minus states, respectively. Gauche states bend the backbone of the polymer. If all torsion angles in the polymer are trans states, its conformation becomes the rod-like zigzag conformation.

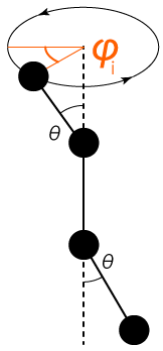

Figure 1.1 Torsion angle

The energy difference between the trans and gauche minima, $\Delta\varepsilon$, is related to the ratio of the number of trans states to that of gauche states. The smaller $\Delta\varepsilon$ is, the more gauche states appear. $\Delta\varepsilon$ defines the static flexibility of the polymer chain. We denote the value of energy barrier between the trans and gauche states by ΔU. ΔU gives the frequency of transition between the trans and gauche states. If ΔU is large, the conformation of a polymer keeps the initial state and looks like "frozen". We study about a polymer of which $\Delta\varepsilon$ and ΔU are so small that we can consider the polymer chain as a long and flexible curve with a finite length.

In order to calculate statistical properties of a polymer chain, we approximate the curve of the polymer chain as a sequence of straight line segments. One of the line segments corresponds to a part of the polymer chain, which has enough gauche states to extinguish the correlation of the polymer direction of the bonds at both ends. We call the length of such a part of a polymer the persistence length.

Random walk model for a linear polymer chain

A random walk on a lattice is one of the models for a linear polymer chain in a solution. The random walk starts at a point on a lattice and jumps to one of the

neighboring points. Each direction of the jump has the same statistical weight. The random walk is the trajectory of a sequence of such steps.

The steps of an ideal random walk does not have any correlation, of which path can cross itself and does not depend on the past steps. An ideal random walk describes the conformation of a single polymer chain in a solvent or a polymer chain in a polymer melt.

Let us consider such a random walk that has some correlation only for a finite interval of time tc. If one of the random walk that have the correlation passes through a given point x(t) at time t, it cannot return to x(t) before time t+tc. Such random walks are almost ideal random walks, since we can put them into ideal random walks with a persistence length tc. If we replace a succession of tc steps with a single step, the sequence of such steps is an ideal random walk.

Conversely, a random walk which never returns to the past points again has different statistical properties from that of ideal random walks. We call such a random walk a Self-Avoiding random Walk (SAW) [5]. The mean square (MS) end-to-end distance of N-step SAW is larger than that of N-step ideal random walks. The distribution function of end-to-end vectors of SAW has the minimum at the origin, whereas that of ideal random walks has the maximum at the origin. In other words, SAW hardly returns to the initial point.

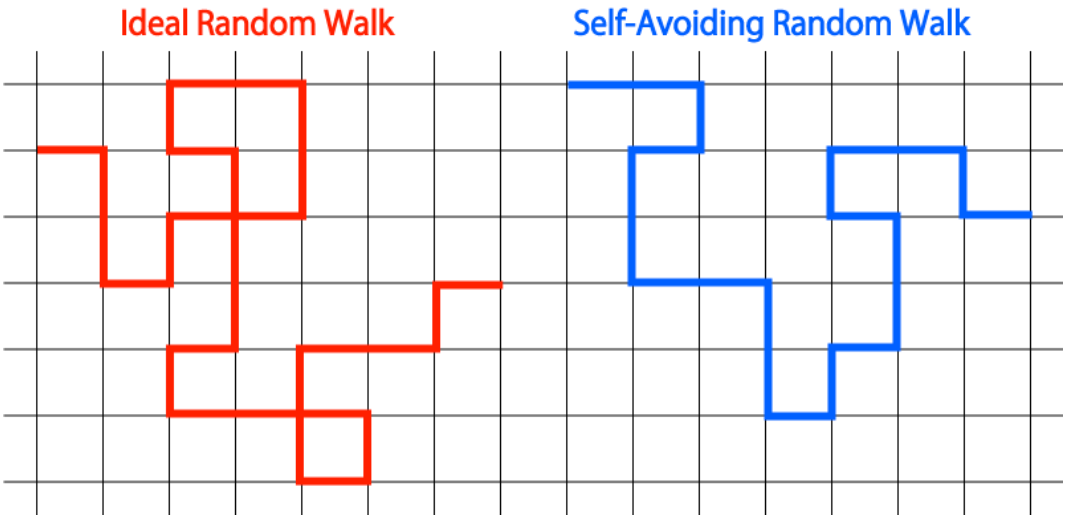

Figure 1.2 An ideal random walk and a self-avoiding random walk

SAW corresponds to a conformation of a polymer chain in dilute solution, whose segment interacts with themselves and molecules of a solvent. A polymer chain swells with molecules of the solvent. The source of swelling is an entropic force which makes

the system tend to be disordered. Swelling becomes effective in the solvent in high temperature because the strength of an entropic force is proportional to the temperature of the system. When the interaction from molecules of the solvent and that of the polymer are balanced, the conformation of the polymer becomes ideal.

Scaling properties of random walks

Define the end-to-end distance as the distance between the initial point and the end point of a random walk:

$$R^2 \equiv |\boldsymbol{r}_N - \boldsymbol{r}_0|^2 = \left(\sum_{i=1}^{N} \boldsymbol{b}_i\right)^2, \tag{1.1}$$

where r_i is the position vector of the i-th segment of the random walk and bi is the i-th step vector defined as $b_i = r_i - r_{i-1}$.

On the basis of the definition of the ideal random walk, the average of the step vectors of ideal random walks are

$$\langle \boldsymbol{b}_k \rangle = 0, \langle \boldsymbol{b}_k^2 \rangle = b^2, \langle \boldsymbol{b}_k \cdot \boldsymbol{b}_{k'} \rangle = b^2 \delta_{kk'}. \tag{1.2}$$

where $\langle A \rangle$ means the average value of A over the ensemble of random polygons.

Therefore, the MS end-to-end distance of ideal random walks is

$$\left\langle \left(\sum_{i=1}^{N} \boldsymbol{b}_i\right)^2 \right\rangle = \sum_{i=1}^{N} \langle \boldsymbol{b}_i^2 \rangle + 2 \sum_{i=1}^{N} \sum_{j=i+1}^{N} \langle \boldsymbol{b}_i \cdot \boldsymbol{b}_j \rangle = Nb^2, \tag{1.3}$$

where b is the average length of the step vectors.

The root mean square (RMS) end-to-end distance of ideal random walks is proportional to the number of steps N.

The end-to-end distance cannot be defined for a non-linear polymer chains such as a ring, branched, or caged polymer chain. We introduce the radius of gyration which is defined as the MS length of the vectors between the center of mass and one of the segments of the polymer chain.

$$R_G^2 \equiv \frac{1}{N+1} \sum_{i=0}^{N} (\boldsymbol{r}_i - \boldsymbol{r}_G)^2 = \frac{1}{(N+1)^2} \sum_{i=0}^{N} \sum_{j=i+1}^{N} \left(\boldsymbol{r}_i - \boldsymbol{r}_j\right)^2. \tag{1.4}$$

The MS radius of gyration for ideal random walks is calculated as follows:

$$
\begin{aligned}
&\langle \frac{1}{(N+1)^2} \sum_{i=0}^{N} \sum_{j=i+1}^{N} (\boldsymbol{r}_i - \boldsymbol{r}_j)^2 \rangle \\
&= \langle \frac{1}{(N+1)^2} \sum_{i=0}^{N} \sum_{j=i+1}^{N} \left(\sum_{l=1}^{i} \boldsymbol{b}_l - \sum_{l=1}^{j} \boldsymbol{b}_l \right)^2 \rangle \\
&= \frac{1}{(N+1)^2} \sum_{i=0}^{N} \sum_{j=i+1}^{N} \sum_{l=i+1}^{j} \langle \boldsymbol{b}_l^2 \rangle \\
&= \frac{1}{(N+1)^2} \sum_{i=0}^{N} \sum_{j=i+1}^{N} (j-i) b^2 \\
&= \frac{b^2}{(N+1)^2} \sum_{i=0}^{N} \frac{1}{2} (i^2 - (1+2N)i + N(N+1)) \\
&= \frac{N(N+2)b^2}{6(N+1)} \cong \frac{N}{6} b^2 .
\end{aligned}
\tag{1.5}
$$

The RMS radius of gyration of ideal random walks is proportional to N as the RMS end-to-end distance of ideal random walks is.

In case of SAW, the exact value of the MS radius of gyration is not obvious since the product of a pair of the step vectors of SAW has non-zero diagonal elements. Numerical results or perturbation series suggest the proportionality between N to the ν-th power and the MS gyration of SAW.

$$
R^2, R_G^2 \propto N^{2\nu}. \tag{1.6}
$$

Statistical properties

The total number of N-step ideal random walks on a lattice is

$$
\mathrm{z}^{\mathrm{N}}, \tag{1.7}
$$

where z is the number of the neighboring sites on the lattice.

The exact number of SAW on a d-dimensional cubic lattice for small N is

$$\begin{aligned}\Re_1 &= 2d,\\ \Re_2 &= 2d(2d-1),\\ \Re_3 &= 2d(2d-1)^2,\\ \Re_4 &= 2d(2d-1)^3 - 2d(2d-2).\end{aligned} \tag{1.8}$$

Since SAW never goes back, the number of the available sites is 2d-1 except for the case of the first step. When N is larger than 3, we subtract correction terms from 2d(2d-1)^(N-1) to remove crossing trajectories. The exact value of correction terms has not been generalized for N.

The numerical result for the number of SAW is approximated by

$$\Re_N \propto \bar{z}^N N^{\gamma-1}, \tag{1.9}$$

where $\bar{z}$ and γ is the constant number which depends on d. This equation grows exponentially when N→∞ as the number of ideal random walks does. However, z ¯ is clearly smaller than z and 2d-1. One of the certain lower limits of $\bar{z}$ is d, which corresponds to the set of SAW which go forward the only positive direction. We show that $\log \Re_N \sim N \log \bar{z}$ for infinite N. Moreover, we can show that $\gamma \geq 1$ if we apply N^(γ -1) for the corrections because $\Re_N \geq \bar{z}^N$.

We show that there is the limit

$$\bar{z} = \lim_{N\to\infty} (\Re_N)^{\frac{1}{N}}. \tag{1.10}$$

Consider concatenation of two SAW. Concatenated random walks are not always self-avoiding:

$$\Re_{N+M} \leq \Re_N \Re_M. \tag{1.11}$$

Then we get subadditive numbers:

$$\log \Re_{N+M} \leq \log \Re_N + \log \Re_M. \tag{1.12}$$

A sequence of some subadditive real numbers, i.e., $a_{N+M} \leq a_N + a_M$, has the limit.

$$\lim_{N\to\infty} \frac{a_N}{N} = \inf \frac{a_N}{N}. \tag{1.13}$$

Proof. Define $A_k \equiv \max a_j$ and j as the largest integer which is less than N/k. N is

equal to jk+r, where r is an integer which is larger than 0 and less than k.

$$a_{jk+r} \leq a_{jk} + a_r.$$
$$a_{jk+r} \leq j a_k + a_r \tag{1.14}$$

Hence

$$a_N \leq j a_k + a_r \leq \frac{N}{k} a_k + A_k.$$
$$\frac{\mathrm{a_N}}{N} - \frac{A_k}{N} \leq \frac{a_k}{k}. \tag{1.15}$$

Taking the limit supremum N→∞, we have

$$\lim_{N\to\infty} \sup \frac{a_N}{N} \leq \frac{a_k}{k} \; for\; every\; k. \tag{1.16}$$

(1.16) gives (1.13).

Therefore we have

$$\lim_{N\to\infty} \frac{\log \mathfrak{R}_N}{N} = \inf \frac{\log \mathfrak{R}_N}{N} \equiv \log \bar{z}. \tag{1.17}$$

We get one of the infima of z ¯

$$\bar{z}^N \leq \mathfrak{R}_N \; for\; every\; N. \tag{1.18}$$

Considering random walks which are self-avoiding only over a finite time scale τ, we obtain a smaller infimum of $\bar{z}$. Obviously, the total number of such random walks is

$$\mathfrak{R}_N \leq \mathfrak{R}_{N,\tau}. \tag{1.19}$$

$\log \mathfrak{R}_N, \tau$ is subadditive as the logarithm of the total number of SAW is. Thus the limit z_τ exists:

$$z_\tau \equiv \lim_{N\to\infty} \left(\mathfrak{R}_{N,\tau}\right)^{\frac{1}{N}}. \tag{1.20}$$

z_τ is one of the infima of $\bar{z}$. As τ increases, z_τ converges on $\bar{z}$.

We can obtain a supremum of $\bar{z}$ from N-step bridges which makes a part of SAW. The position vector r_i of the i-th segment of an N-step bridge has a component which satisfies

$$r(0) < r(i) \leq r(j), when\ i \leq j. \tag{1.21}$$

The total number of N-step bridges $\mathfrak{R}_{\mathrm{b}}(N)$ satisfies the following inequalities:

$$\mathfrak{R}_b(N)\mathfrak{R}_b(M) \leq \mathfrak{R}_b(N+M). \tag{1.22}$$

Since $-\log \mathfrak{R}_b(N)$ is subadditive, we have

$$z_b \equiv \lim_{N\to\infty} \left(\mathfrak{R}_b(N)\right)^{\frac{1}{N}} = (\sup \mathfrak{R}_b(N))^{\frac{1}{N}}. \tag{1.23}$$

z_b is one of the suprema of $\bar{z}$. Therefore

$$z_b \leq \bar{z} \leq z_\tau. \tag{1.24}$$

We show some numerical result for $\bar{z}$ [5]:

d	Estimate
2	$\bar{z} = 2.6381585 \pm 0.000001$
3	$\bar{z} = 4.6839066 \pm 0.0002$
4	$\bar{z} = 6.7720 \pm 0.0005$

2 Numerical methods

2.1 Random polygon model for a knotted polymer

Random polygon model

We study the knot probability of ring polymers through simulation of off-lattice self-avoiding random polygon (SAP) consisting of cylinders with radius r. The length of the cylinders which we fixed it by 1, corresponds to the persistent length of a DNA molecule. The number of the cylinders of SAP is proportional to the number of the base pairs of the DNA molecule. The radius of the cylinders is an analogy to the effective diameter of the DNA molecule that is surrounded by counter ions; it expresses the shielding effect of counter ions [41]. In this paper, we show that the knot probability depends on the number and radius of the cylinders of SAP and these two parameters describe knotted DNA in various environments.

2.2 SAP Generation

Crank-shaft algorithm

We generate an ensemble of SAP consisting of N cylindrical segments with radius r through the Monte-Carlo method as follows: First, we have an equilateral regular N-gon for the initial states. Secondly, we choose two vertices of the N-gon randomly. And we rotate the segments between these vertices around the line between them by a degree chosen randomly from 0 to 2π. Thirdly, we check whether the rotated segments have overlaps with the remaining segments or not. However, we do not check overlaps of the pairs of neighboring segments. If they have any overlap, namely, the polygon has some overlap, we employ the old polygon before the latest rotation for the next Monte-Carlo step. If not, we employ the rotated one. Then we repeat these rotating and checking procedures 2N times. After that, we add the last configuration to the ensemble of SAP as shown in fig. 2.1.

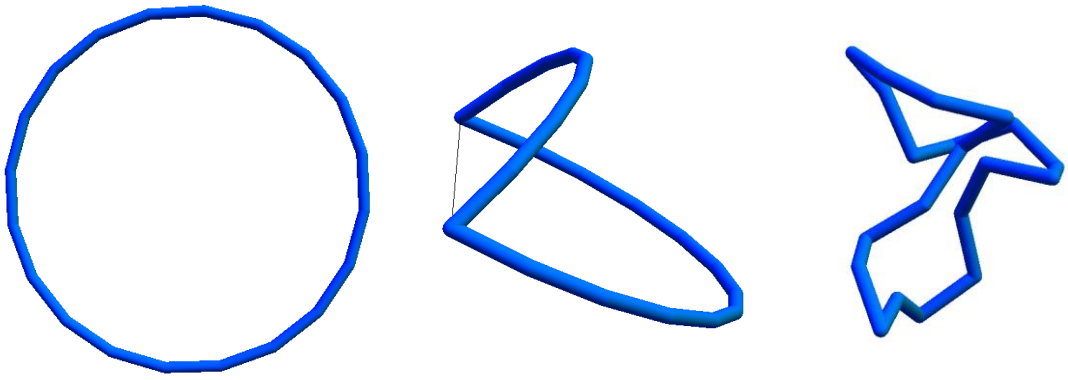

Initial polygon After rotation SAP

Figure 2.1 Crank-shaft method

Computational flexibility

The computational time of the algorithm is proportional to N^2. The rotation process takes a time interval proportional to N. However, most of the total computational time is spent for checking overlaps among segments. In fact, the computational time is much shorter for generating random polygons without excluded volume. If we check overlaps over all pairs of the segments of the polygon, it takes a time proportional to N^2. Moreover, the entire computational time is proportional to N^3 because the rotating and checking process is repeated 2N times in the program. Thus we check overlaps by using the bucket sort whose computational complexity is given by N.

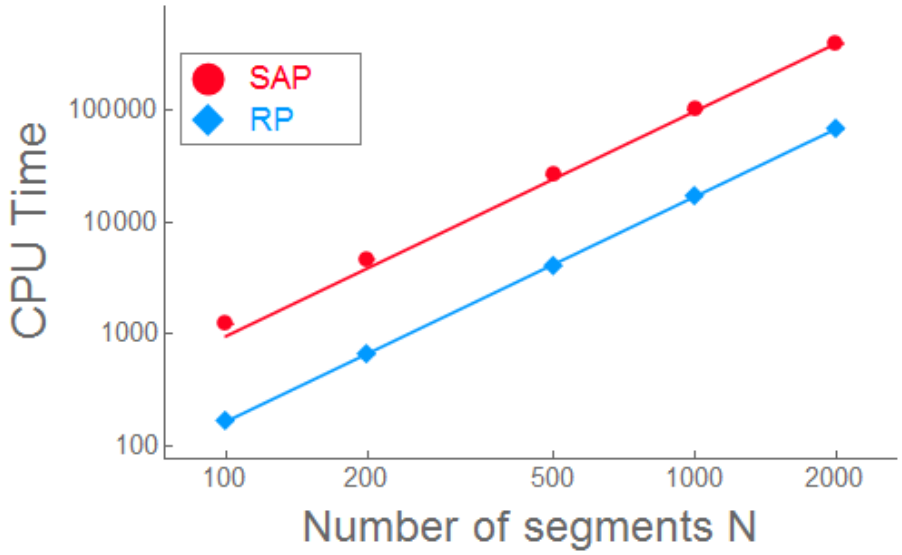

Figure 2.2 Computational times to generate random polygons are plotted against the number of segments of the polygons in double-logarithmic scale. The fitting curves are given by cN^2.

Fig. 2.2 shows the CPU times for generation of SAP and RP with different values of N in the double logarithmic scale. Here we used a workstation produced by HPC systems. The CPU times are proportional to N^2 for both SAP and RP, however, the CPU time for generating SAP is about 10 times as large as that for RP.

Estimates of knot probability

Now we explain how we evaluated the knot probability of a given knot K in a model of RP or SAP.

We denote by M(N,r) the number of RP or SAP in the ensemble of generated SAP or RP of N segments with cylindrical radius r, where r is equal to 0 for RP. The value of M(N,r) is given in the next section. We define the number of SAP or RP with knot K in the ensemble by $M_K(N, r)$.

We evaluated the knot probability of knot K by

$$P(N;r,K) = \frac{M_K(N,r)}{M(N,r)}. \tag{2.1}$$

And we assumed that $M_K(N,r)$ follows the binomial distribution. Hence the variance of $M_K(N, r)$ is estimated by

$$V[M_K(N,r)] = M(N,r)P(N;r,K)(1 - P(N;r,K)). \tag{2.2}$$

Thus the standard error of the knot probability is

$$\mathrm{SE}\big(\mathrm{P(N;r,K)}\big) = \frac{\sqrt{M_K(N,r)(1-P(N;r,K))}}{\mathrm{M(N,r)}} \sim \frac{\sqrt{M_{K(N,r)}}}{M(N,r)}. \qquad (2.3)$$

We approximated the standard errors of the knot probability given by the right term of the equation (2.3).

In the next section, we explain how we can detect the knot type of a given SAP. We use the two knot invariants: One is the absolute value of Alexander polynomial $\Delta_{\mathrm{K}}(t)$, evaluated at t=-1; The other is the Vassiliev invariant of the second order $\mathrm{v}_2(K)$.

2.3 Knot invariants

Knot diagram

The knot diagram is the projection of a knotted curve on a plane. No crossing point has 3 or more line on it. In the knot diagram, an undercrossing line segment will be cut at its crossing point in order to recognize which line segment is undercrossing or overcrossing.

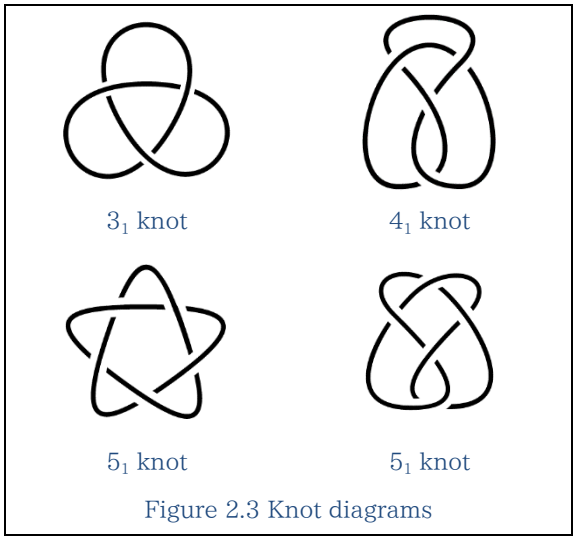

Figure 2.3 Knot diagrams

The knot diagram is not useful to identify the knot type of the curve. One knot has an infinite number of projections which look like different. There are knot diagrams among which the number of crossings is smaller than that of any other knot diagrams for the same topology. Such a number of crossings is called the minimal crossing number.

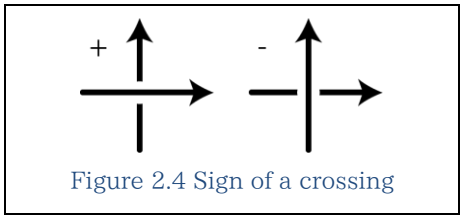

Figure 2.4 Sign of a crossing

We call the topology of which the minimal crossing number is given by 3 the 3_1 knot. Here subscript 1 expresses that the knot is the first one of the knots with the minimal crossing number 3. We show the knot diagrams for the knots whose minimal crossing numbers are less than or equal to 5 in fig. 2.3.

We choose a direction of the curve and call it an oriented knot diagram. The two types of crossing exist in the oriented knot diagram. One of them is called plus and the other minus as shown in fig. 2.4.

Reidemeister moves

Let us explain the 3 types of the Reidemeister moves. The type I move twists or untwists a given single line. The type II move changes a pair of overlapping lines where one line is completely under the other line, into a pair of non-overlapping independent lines. The type III move shifts a line completely under (or over) a pair of crossing lines. Fig. 2.5 shows the 3 types of the Reidemeister moves.

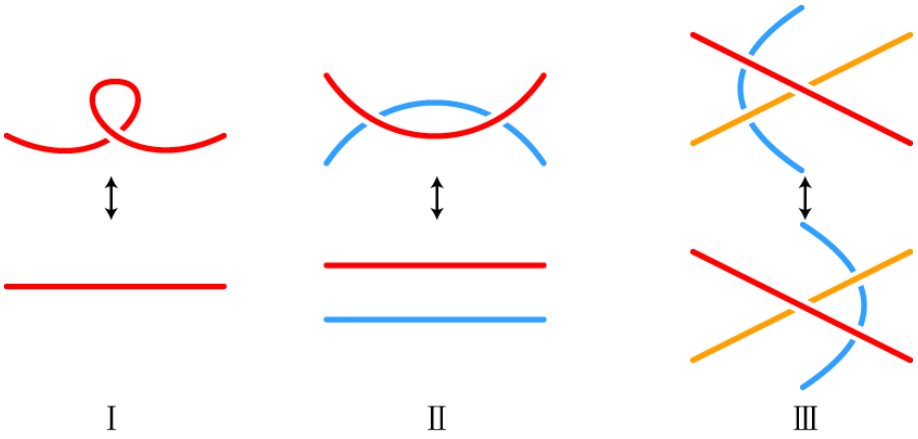

Figure 2.5 The 3 types of the Reidemeister moves

The Reidemeister moves does not change the topology of a closed curve. We call the value that is constant under Reidemeister moves the knot invariant.

The type I and II clearly reduce the number of the crossings of the knot diagram. The type III does not always reduce it. Therefore we do only the type I and II in the simulation to reduce the computer time for calculation of knot invariants.

Gauss code

The gauss code is one of useful ways which represent a knot diagram without drawing the curve of the knot. Choose an arbitrary point and a direction on the oriented knotting curve. Trace the curve from the point and give a number when we underpass or overpass the line. After that, each of the crossing points has a pair of the numbers. Make a sequence whose i-th element has the counterpart number for the i-th crossing point. The gauss code is defined by the sequence of the i-th elements of the sequence for i=1, 3, 5, ⋯

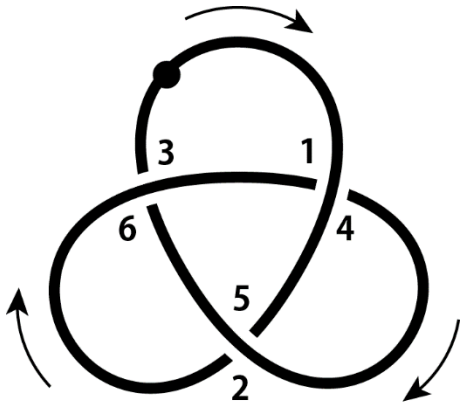

Figure 2.6 Making a gauss code for the right-handed 3_1 knot

For example, in the figure we give numbers from 1 to 6 the crossing points on the 3_1 knot and obtain the Gauss code:

$$(4, 5, 6, 1, 2, 3) \rightarrow (4, 6, 2).$$

If we add the information of the signs of the crossings of the knot, the Gauss code

includes all information of the knot diagram. One of easy methods to represent them is given by the signs of the numbers of the crossings:

$$(+4, +6, +2).$$

We can reconstruct the knot diagram from the gauss code:

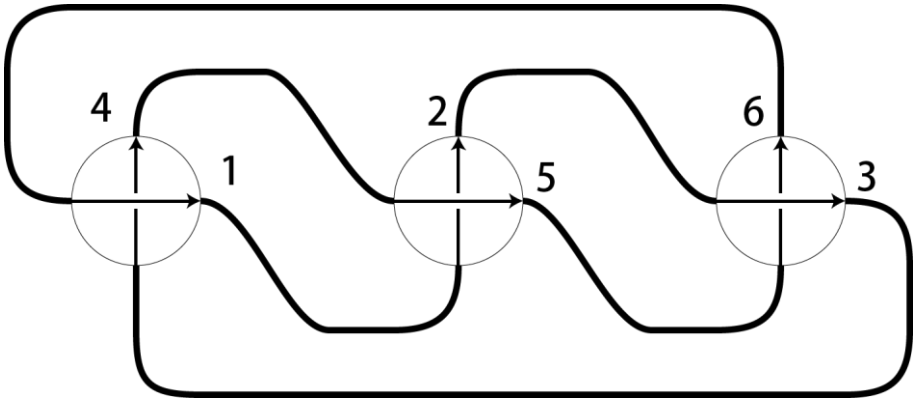

Figure 2.7 Reconstruction of the knot diagram

It is remarkable that a given Gauss code is not unique to the knot. The knot can be represented with several Gauss codes. However, different knots never have the same Gauss code. Since the Gauss code is just a vector of integers, it is easy to operate in a computer. Hence we use the Gauss code and the information of the signs of crossings to calculate knot invariants.

2nd order Vassiliev invariant

We briefly explain how we get the 2nd order Vassiliev invariant $v_2(K)$ of polygons from the Gauss code for the right-handed 3_1 knot. Put the numbers of the crossing points on a circle in sequence anticlockwise. Connect the pair of numbers corresponding to a given crossing point by a chord with an arrow. The arrowed line starts at the number corresponding to the overpassing line segment and end at that to the undercrossing line segment. Add the origin on the circle as a black point. We obtain the Gauss diagram of the knot as shown in fig. 2.8.

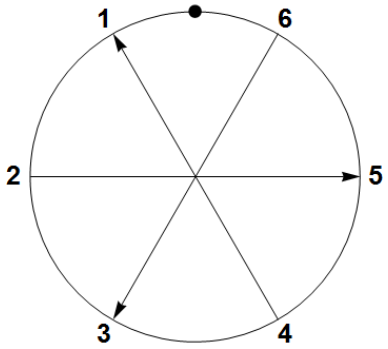

Figure 2.8 Gauss diagram for the right-handed 3_1 knot

We search for such a pair of arrowed lines that cross each other and have the origin between their arrowheads as shown in the following figure.

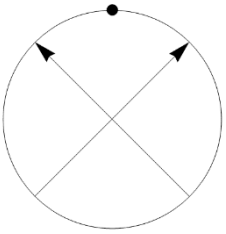

Figure 2.9

Since each arrowed line expresses the crossing in the Gauss diagram, it has the sign of the crossing. Multiply the signs of the pair of crossing arrowed lines. The value of $v_2(K)$ is given by the summation of these products [7]. The 2nd order Vassiliev invariant of the 3_1 knot is given by 1.

Remark that we cannot distinguish between a right-handed knot and the left-handed knot by $v_2(K)$; we need the 3rd order Vassiliev invariant or another invariant for them.

Alexander polynomial

Consider a knot diagram of the 4_1 knot as an example for constructing Alexander polynomial $\Delta_K(t)$ as shown in fig. 2.10. We cut the curve of the knot diagram under the crossing points; give ordering numbers to every segment and every crossing point in sequence. We give one number to one crossing point; the ordering numbers are different from the numbers in the knot diagram, where we gave a pair of numbers to a crossing point.

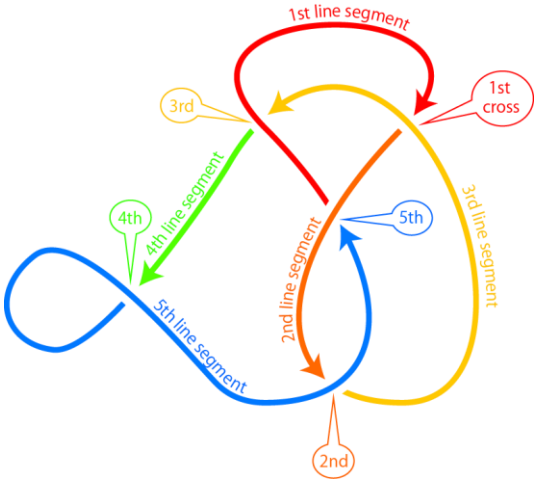

Figure 2.10 Making the Alexander polynomial

We make the Alexander matrix of which the determinant defines the Alexander polynomial. The k-th row of the matrix corresponds to the k-th crossing point. The k-th crossing point has the overpassing line segment numbered by i. An element of the matrix a_{ki} is defined as follows.

If k is equal to i or i-1,

$$a_{kk} = -1, a_{kk+1} = 1. \tag{2.4}$$

If the sign of the k-th cross is plus and k is not equal to i nor i-1,

$$a_{kk} = 1, a_{kk+1} = -t, a_{ki} = t - 1. \tag{2.5}$$

If the sign of the k-th cross is minus and k is not equal to i nor i-1,

$$a_{kk} = -t, a_{kk+1} = 1, a_{ki} = t - 1. \tag{2.6}$$

Every element that has other indices is 0.

Then we get the Alexander matrix for the figure:

$$\begin{pmatrix} -t & 1 & t-1 & 0 & 0 \\ 0 & 1 & -t & 0 & t-1 \\ t-1 & 0 & -t & 1 & 0 \\ 0 & 0 & 0 & -1 & 1 \\ -t & t-1 & 0 & 0 & 1 \end{pmatrix} \tag{2.7}$$

and calculate the Alexander polynomial as the determinant [8]:

$$\Delta_K(-t) = 1 - 3t + t^2. \tag{2.8}$$

Substitute -1 for t,

$$\Delta_K(-1) = 1 \; for \; the \; 3_1 \; knot. \tag{2.9}$$

Values of the knot invariants $\Delta_K(-1)$ and $v_2(K)$

We conclude this section with a table that shows the values of the two knot invariants for the prime knots whose minimal crossing numbers are less than or equal to 7. Notice some knots has the same value of a knot invariant; this is the reason why we use the two knot invariants.

K	$\lvert\Delta_K(-1)\rvert$	$v_2(K)$	K	$\lvert\Delta_K(-1)\rvert$	$v_2(K)$	K	$\lvert\Delta_K(-1)\rvert$	$v_2(K)$
0_1	1	0	6_1	9	-2	7_3	13	5
3_1	3	1	6_2	11	-1	7_4	15	4
4_1	5	-1	6_3	13	1	7_5	17	4
5_1	5	3	7_1	7	6	7_6	19	1
5_2	7	2	7_2	11	3	7_7	21	-1

The value of the 2nd order Vassiliev invariant of the composite knot is given by the summation over those of the included prime knots. For example, it is 0 for $3_1\#4_1$ knot. The value of $\Delta_K(-1)$ of the composite knot is the product over those of the included prime knots. The value of $\Delta_K(-1)$ of the $3_1\#4_1$ knot is 15.

2.4 Conditions of the simulation

We generate SAP with cylindrical radius r given from 0 to 0.06. The number of generated SAP and its number of segments N is shown by the following table.

N	r=0	r=0.005	r=0.01	r=0.02	r=0.03	r=0.04	r=0.05	r=0.06
100	2×10^5	2×10^5	2×10^5	2×10^5	2×10^5	2×10^5	2×10^5	2×10^5
150								
200	2×10^5	2×10^5	2×10^5	2×10^5	2×10^5	2×10^5	2×10^5	2×10^5
250								
300	2×10^5	2×10^5	2×10^5	2×10^5	2×10^5	2×10^5	2×10^5	2×10^5
400	2×10^5	2×10^5	2×10^5	2×10^5	2×10^5	2×10^5	2×10^5	2×10^5
500	2×10^5	2×10^5	2×10^5	2×10^5	2×10^5	2×10^5	2×10^5	2×10^5
600	2×10^5	2×10^5	2×10^5	2×10^5	2×10^5	2×10^5	2×10^5	2×10^5
700	2×10^5	2×10^5	2×10^5	2×10^5	2×10^5	2×10^5	2×10^5	2×10^5
800	2×10^5	2×10^5	2×10^5	2×10^5	2×10^5	2×10^5	2×10^5	2×10^5
900	2×10^5	2×10^5	2×10^5	2×10^5	2×10^5	2×10^5	2×10^5	2×10^5
1000	2×10^5	2×10^5	2×10^5	2×10^5	2×10^5	2×10^5	2×10^5	2×10^5
1100	2×10^5	2×10^5	2×10^5	2×10^5	2×10^5	2×10^5	2×10^5	2×10^5
1200	2×10^5	2×10^5	2×10^5	2×10^5	2×10^5	2×10^5	2×10^5	2×10^5
1300	2×10^5	2×10^5	2×10^5	2×10^5	2×10^5	2×10^5	2×10^5	2×10^5
1400	2×10^5	2×10^5	2×10^5	2×10^5	2×10^5	2×10^5	2×10^5	2×10^5
1500	2×10^5	2×10^5	2×10^5	2×10^5	2×10^5	2×10^5	2×10^5	2×10^5
1600	2×10^5	2×10^5	2×10^5	2×10^5	2×10^5	2×10^5	2×10^5	2×10^5
1800	2×10^5	2×10^5	2×10^5	2×10^5	2×10^5	2×10^5	2×10^5	2×10^5
2000	2×10^5	2×10^5	2×10^5	2×10^5	2×10^5	2×10^5	2×10^5	2×10^5
2200		2×10^5	2×10^5	2×10^5	2×10^5	2×10^5	2×10^5	2×10^5
2400		2×10^5	2×10^5	2×10^5	2×10^5	2×10^5	2×10^5	2×10^5
2600			2×10^5	2×10^5	2×10^5	2×10^5		
3000				2×10^5	2×10^5	2×10^5	2×10^5	2×10^5
3500				2×10^5	2×10^5	2×10^5	2×10^5	
4000				2×10^5	2×10^5	2×10^5	2×10^5	2×10^5
4500					10^5	10^5	10^5	10^5
5000					10^5	10^5	10^5	10^5
5500						10^5	10^5	10^5
6000						10^5	10^5	10^5
6500						5×10^4	5×10^4	5×10^4
7000						5×10^4	5×10^4	5×10^4
7500							5×10^4	5×10^4
8000							5×10^4	5×10^4
9000								4×10^4
10000								4×10^4

Since the computational time for generating SAP is proportional to N^2, the possible

number of SAP is limited for large N.

We detect the 217 types of knots: the trivial knot, the prime knots of which the minimal crossing numbers are below 7, and some composite knots. Some knots have the same values in the $v_2(K)$ and $|\Delta_K(-1)|$. For example, both the knot 7_4 and the knot $3_1\#5_1$ have the value of $v_2(K) = 4$ and $|\Delta_K(-1)| = 15$. Therefore we cannot distinguish them. We evaluate the 3rd order Vassiliev invariants for such polygons whose $v_2(K) = 4$ and $|\Delta_K(-1)| = 15$.

3 Knot probability

3.1 Formula for the knot probability

Localization of a knot

Consider a subchain that is part of a knotted polygon consisting of N segments with knot type K. Connecting the both ends of the subchain, we obtain a small polygon with n_1 segments. Some of such small polygons have the same knot type K. We define n_Kmin as the minimum value of n_1 of the small polygons that have the knot type K from the original polygons. If the value n_Kmin/N is close to 0, we assume that the knot is localized. If not, the entanglement of the knot is un-localized.

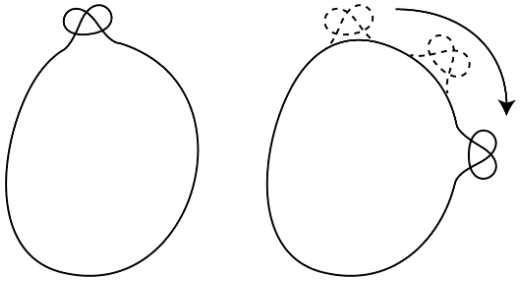

Figure 3.1 Moving localized knot

Since a localized knot can move over the polygon, we expect that the knot probability of a prime knot is the product of the number of vertices N and some kind of functions that illustrates the decrease of the knot probability of the prime knot for large N. A composite knot includes several prime knots; they are independent each other and can move freely. It has a degree of freedom proportional to N to the m-th power, where m is the number of included prime knots in the composite knot.

Previous research for the knot probability

In previous researches, the knot probability have been fitted by the following formula [21, 22, 28, 29]:

$$\mathrm{P(N;r,K)} = \mathrm{C_K}\tilde{N}^{m(K)}\mathrm{Exp}\left(-\tilde{N}\right), \tag{3.1}$$

where $\tilde{N}$ is given by

$$\tilde{N} = \frac{N - N_{ini}}{N_K}. \tag{3.2}$$

This formula has the 4 fitting parameters: C_K, m(K), N_K, and Nini(K). The coefficient C_K is associated with the maximum value of the knot probability as a function of N, which depends on both r and K. We call N_K the characteristic length of random

knotting of SAP, which depends on the radius of cylinders r. The parameter Nini gives finite-size corrections. When N is small, the exact form of knot probability as a function of N is not known. However, Nini gives good fitting curve to the simulation results, where the Chi-squared values of the fitting are small enough. Thus it is concluded that the formula well explained the behavior of knot probabilities in the previous researches.

By fitting an asymptotic formula to the knot probabilities of a prime knot of on-lattice polygons, it was find that the m(K) is close to 1. For a composite knot, m(K) is close to the number of constituent prime knots m. It suggests that N^m(K) in the number of knot is related with moving of a localized knot.

However, m(K) is less than m for the knot probability of the off-lattice polygons. The estimated m(K) is clearly smaller than m if we cut the data points of polygons with large N. m(K) is close to m for the knot probability of polygons of which the number of segment N is smaller than NK. It is contradictory results to our prospect that localization of the knot in a polygon dominates as N becomes larger.

New formula for knot probability

The formula of the knot probability is derived from the expansion of the Gamma function. We add the higher terms to the formula:

$$\begin{aligned}\mathrm{Log}\big(\mathrm{P(N;r,K)}\big) &= \mathrm{Log}(C_K) + m(K)\,\mathrm{Log}\left(\frac{N}{N_K}\right) \\ &- \frac{N}{N_K} + b_1\left(\frac{N}{N_K}\right)^{-1} - b_3\left(\frac{N}{N_K}\right)^{-3} + O(N^{-5})\end{aligned} \tag{3.3}$$

bn is defined by

$$\mathrm{b_n} = \frac{B_{n+1}}{n(n+1)}. \tag{3.4}$$

where Bn is the n-th Bernouilli number defined by

$$\frac{\mathrm{x}}{\mathrm{e^x} - 1} = \sum_{n=0}^{\infty} \frac{B_n}{n!} x^n. \tag{3.5}$$

Taking exponential of the equation (3.3), we obtain a new formula for knot probabilities:

$$\mathrm{P(N;r,K)} = \mathrm{C_K}\left(\frac{N}{N_K}\right)^{m(K)} \mathrm{Exp}\left(-\frac{N}{N_K}+\frac{N_K}{12N}-\frac{N_K^3}{360N^3}\right). \quad (3.6)$$

The finite-size correction, Nini, is not necessary for (3.6) if $\mathrm{N} \geq \mathrm{N_K}$. Although (3.6) seems to be more complex than the formula (3.1), the formula (3.6) has only 3 parameters. Also we can express the knot probability by Gamma function:

$$\mathrm{P(N;r,K)} = \frac{\mathrm{C_K} x^{m(K)-1/2-x}\Gamma(x+1)}{\sqrt{2\pi}}, \quad (3.7)$$

where x is $\mathrm{N/N_K}$. In the previous equation, we use the expanded Gamma function:

$$\mathrm{Log}\left(\frac{\Gamma(x+1)}{x^x\sqrt{2\pi x}}\right) = -x+\frac{1}{12x}-\frac{1}{360x^3}+O(x^{-5}). \quad (3.8)$$

This form gives a good fitting curves for an asymptotical region of knot probabilities.

3.2 Knot probability for prime knots

The knot probabilities whose minimal crossing numbers are less than or equal to 6 are plotted against the number of segments N in the figure 3.2. The fitting curves are given by formula (3.8) for different values of the cylindrical radius r.

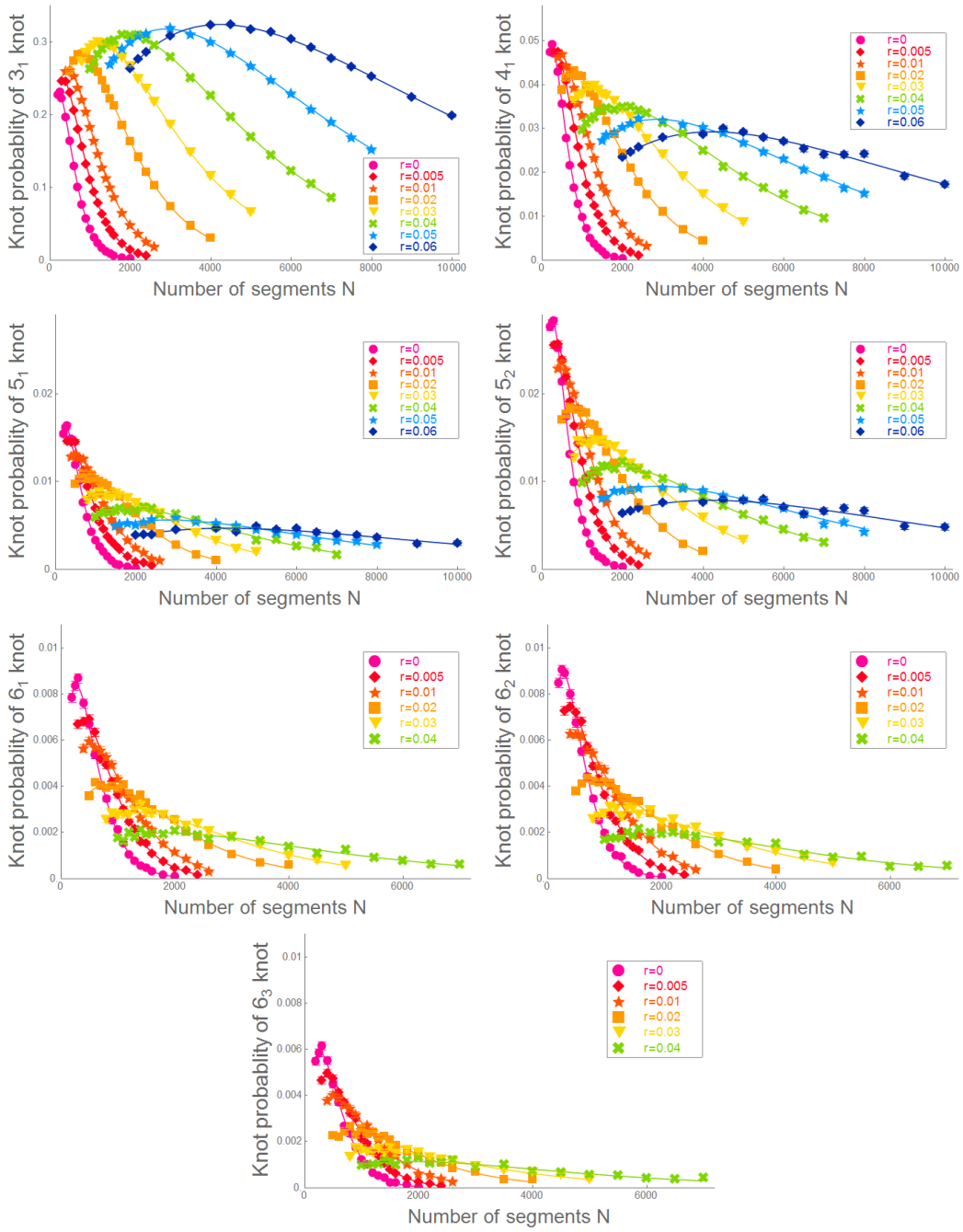

Figure 3.2 Knot probabilities for the prime knots whose minimal crossing numbers are below 7 is plotted against the number of segments of RP or SAP.

The maximum value of the knot probability of the 3_1 knot increases as cylindrical radius r increases. It is only happened for the case of the 3_1 knot. In contrast, the maximum values of the other prime knots, the 4_1, 5_1, 5_2, 6_1, 6_2 and 6_3 knots decrease as r increases. For the same cylindrical radius r, the number of segments which gives the maximum value of the knot probability of any prime knot are equal.

For the knots with the same crossing number and the same cylindrical radius r, the maximum values of the knot probabilities are sometimes different. We know that the knot probability of the 5_1 knot are smaller than that of the 5_2 knot [29]. We also found that the knot probabilities of the 6_1 and 6_2 knots, they are very similar, are larger than that of the 6_3 knot.

The best estimates of the fitting parameters and χ^2 value per degree of freedom (χ^2/DF) are listed in the following tables:

For knot 3_1:

	C_K		m(K)		N_K		χ^2/DF
r=0	0.5749 ± 0.0015		1.005 ± 0.012		249 ± 1.4		1.16
r=0.005	0.6192 ± 0.002		0.972 ± 0.015		368.7 ± 2.6		1.73
r=0.01	0.6532 ± 0.0016		0.989 ± 0.012		500.3 ± 3.1		1.24
r=0.02	0.7056 ± 0.0012		1.0237 ± 0.0088		835 ± 4.6		1.34
r=0.03	0.74562 ± 0.00098		1.0624 ± 0.0094		1290.3 ± 8.2		1.07
r=0.04	0.7753 ± 0.001		1.0813 ± 0.0082		1942 ± 13		1.09
r=0.05	0.79592 ± 0.00097		1.0947 ± 0.0083		2846 ± 21		0.6
r=0.06	0.81125 ± 0.00096		1.0972 ± 0.0079		4139 ± 34		0.38

For knot 4_1:

	C_K		m(K)		N_K		χ^2/DF
r=0	0.12165 ± 0.00082		1.061 ± 0.028		245.4 ± 3.2		1.47
r=0.005	0.11987 ± 0.00074		0.993 ± 0.027		365 ± 4.6		1.13
r=0.01	0.11671 ± 0.00076		1.033 ± 0.031		484 ± 7.5		1.41
r=0.02	0.10636 ± 0.00038		1.045 ± 0.019		820.1 ± 9.5		0.93
r=0.03	0.09723 ± 0.00039		1.003 ± 0.024		1328 ± 22		0.93
r=0.04	0.08758 ± 0.00035		1.065 ± 0.023		1954 ± 37		0.97
r=0.05	0.08034 ± 0.00034		1.082 ± 0.028		2846 ± 70		0.67
r=0.06	0.07302 ± 0.00044		1.146 ± 0.05		3930 ± 190		1.32

For knot 5_1:

	C_K		m(K)		N_K		χ^2/DF
r=0	0.04041 ± 0.00047		1.137 ± 0.045		242.9 ± 5		1.32
r=0.005	0.03725 ± 0.00056		0.99 ± 0.067		370 ± 12		2.22
r=0.01	0.03289 ± 0.00032		1.113 ± 0.042		475.2 ± 9.7		0.73
r=0.02	0.02664 ± 0.00023		1.098 ± 0.046		801 ± 22		1.38
r=0.03	0.02127 ± 0.00016		1.058 ± 0.052		1282 ± 45		0.94

r=0.04	0.01724	±	0.00021	1.031	±	0.063	1970	±	100	1.42
r=0.05	0.01401	±	0.00023	1.007	±	0.074	3010	±	210	0.84
r=0.06	0.0117	±	0.00016	1.12	±	0.1	4060	±	430	0.93

For knot 5_2:

	C_K			m(K)			N_K			χ^2/DF
r=0	0.07089	±	0.00055	1.15	±	0.03	237.5	±	3.1	0.92
r=0.005	0.06445	±	0.00054	1.066	±	0.034	355	±	5.5	0.97
r=0.01	0.0585	±	0.00046	1.044	±	0.037	481	±	8.9	0.99
r=0.02	0.04602	±	0.00026	1.041	±	0.03	819	±	15	0.98
r=0.03	0.03644	±	0.00028	1.07	±	0.055	1282	±	48	1.78
r=0.04	0.02932	±	0.00019	1.08	±	0.039	1904	±	59	0.92
r=0.05	0.02369	±	0.00021	1.065	±	0.052	2920	±	140	0.7
r=0.06	0.01967	±	0.00027	1.112	±	0.099	4050	±	400	1.41

For knot 6_1:

	C_K	m(K)	N_K	χ^2/DF
r=0	0.0209 ± 0.00028	1.143 ± 0.052	252.1 ± 6	0.97
r=0.005	0.01724 ± 0.00033	1.174 ± 0.068	354 ± 11	1.13
r=0.01	0.01454 ± 0.00026	1.219 ± 0.064	453 ± 13	0.77
r=0.02	0.01012 ± 0.00014	1.027 ± 0.074	849 ± 39	1.34
r=0.03	0.00716 ± 0.0001	1.207 ± 0.088	1156 ± 62	0.88
r=0.04	0.00494 ± 0.00012	1.01 ± 0.11	2020 ± 190	1.3

For knot 6_2:

	C_K	m(K)	N_K	χ^2/DF
r=0	0.02217 ± 0.00034	1.183 ± 0.056	240.3 ± 5.9	1.12
r=0.005	0.0188 ± 0.00032	1.111 ± 0.066	351 ± 11	1.08
r=0.01	0.01575 ± 0.00029	1.074 ± 0.082	480 ± 19	1.36
r=0.02	0.01058 ± 0.00012	1.071 ± 0.062	806 ± 30	0.98
r=0.03	0.00727 ± 0.00012	1.1 ± 0.12	1260 ± 100	1.69
r=0.04	0.004943 ± 0.000076	1.15 ± 0.11	1750 ± 150	1.24

For knot 6_3:

	C_K	m(K)	N_K	χ^2/DF
r=0	0.01468 ± 0.00029	1.172 ± 0.074	242.3 ± 8	1.28
r=0.005	0.01199 ± 0.0003	1.247 ± 0.076	325 ± 10	0.88
r=0.01	0.00981 ± 0.00025	1.11 ± 0.11	472 ± 25	1.43
r=0.02	0.00617 ± 0.00012	1.11 ± 0.11	794 ± 50	1.59
r=0.03	0.003988 ± 0.000085	1.06 ± 0.15	1290 ± 130	1.47
r=0.04	0.002846 ± 0.000069	1.09 ± 0.16	1880 ± 230	1.37

For the 3_1 knot, the value of the coefficient C_K increases as r grows. For the other knots, it decreases as r grows. Since the coefficient C_K is proportional to the maximum value of the knot probability of knot K, this result agrees with the fact that the maximum value of the knot probability of the 3_1 knot increases and those of the other

knots decreases as r increases. The values of N_K for different types of knots are almost same. The exponents m(K) are close to 1 for any prime knot or any cylindrical radius r.

The values of χ^2/DF are enough small and the residuals of the fittings over standard errors disperse randomly. In the following figures, we show the values of fitting residuals over standard errors.

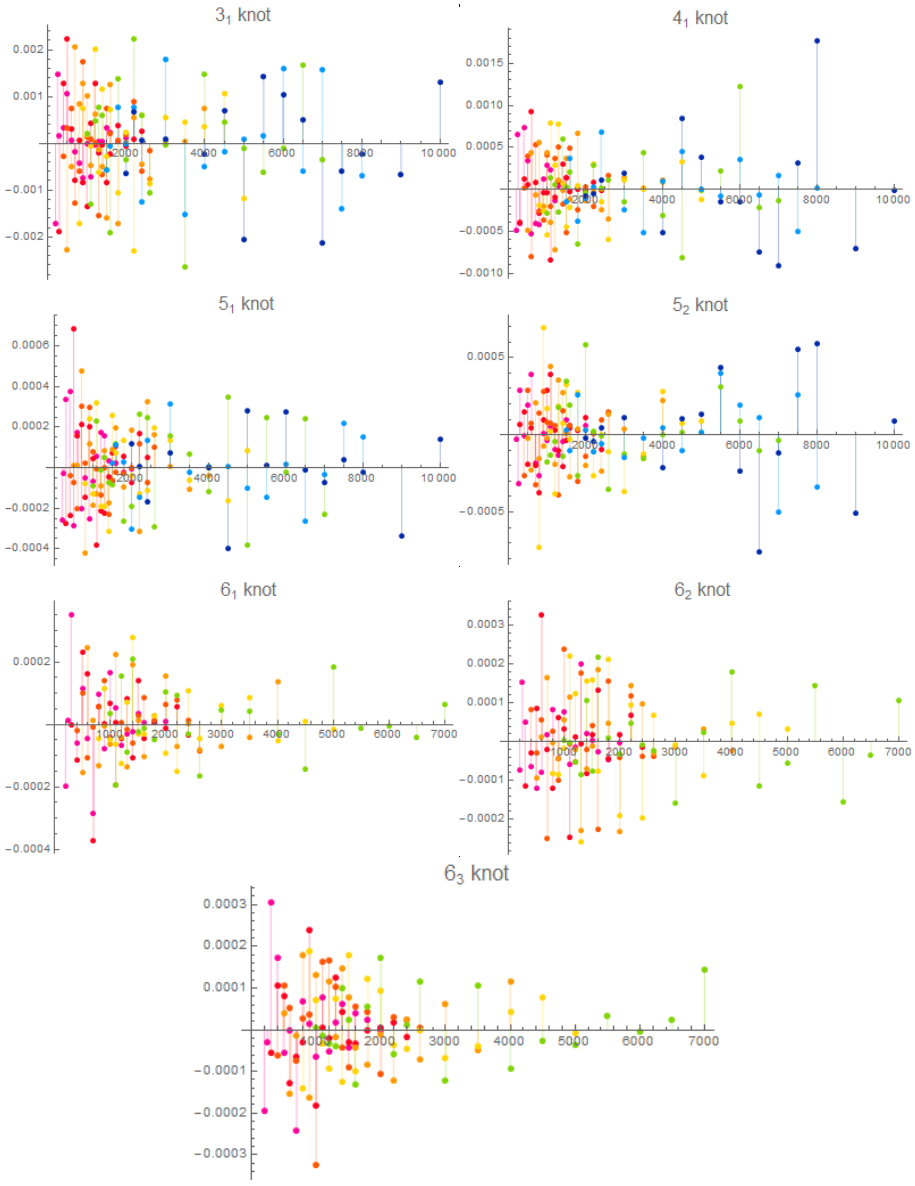

Figure 3.3 Fit residuals over the standard errors

Characteristic length N_K

The estimated N_K are almost same for any knot type K. In the following figure, the characteristic length N_K are plotted against cylindrical radius r in the semi-logarithmic scale for the prime knots whose minimal crossing numbers are below 7.

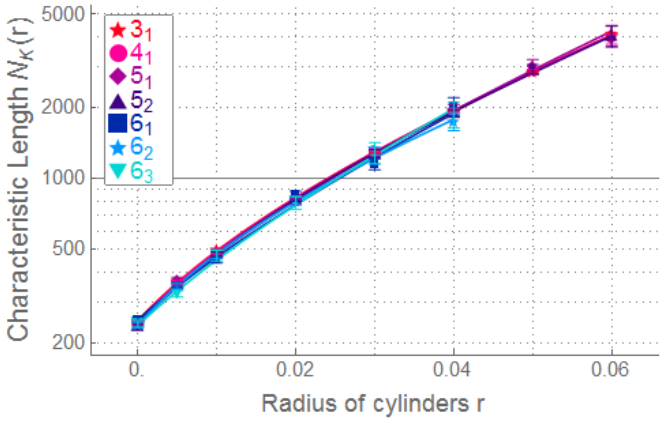

Figure 3.4 Characteristic length N_K for the prime knots are plotted against the cylindrical radius r in the logarithmic scale.

The semi-logarithmic plot of the estimated N_K is approximately straight but is slightly bending and upper convex. Thus we approximated the characteristic length N_K in terms of an exponential function of r with a constant as follows.

$$N_K(r) = c_0 + c_1 Exp(d_1 r). \tag{3.9}$$

The best estimates of c_0, c_1 and d_1 and the value of χ^2/DF is shown in the following table. The fitting curves are good from the viewpoint of the χ^2/DF values.

	c_0	c_1	d_1	χ^2/DF
3_1 knot	-390 ± 21	641 ± 20	32.4 ± 0.56	2.7
4_1 knot	-389 ± 41	636 ± 39	32.5 ± 1.2	1.25
5_1 knot	-314 ± 51	559 ± 49	35 ± 1.9	0.68
5_2 knot	-405 ± 29	643 ± 29	32.25 ± 0.94	0.3
6_1 knot	-210 ± 150	460 ± 150	37.9 ± 7.9	2.12
6_2 knot	-506 ± 54	746 ± 53	28.1 ± 1.5	0.07
6_3 knot	-190 ± 100	425 ± 99	40.9 ± 6.1	0.71

Coefficient C_K

In the figure 3.5, the coefficients C_K of the prime knots are plotted against the cylindrical radius r in the semi-logarithmic scale. The estimated C_K for the prime knots except the case of the 3_1 knot decrease exponentially as r increases and the slope of the semi-logarithmic plot decreases as the minimal crossing number grows.

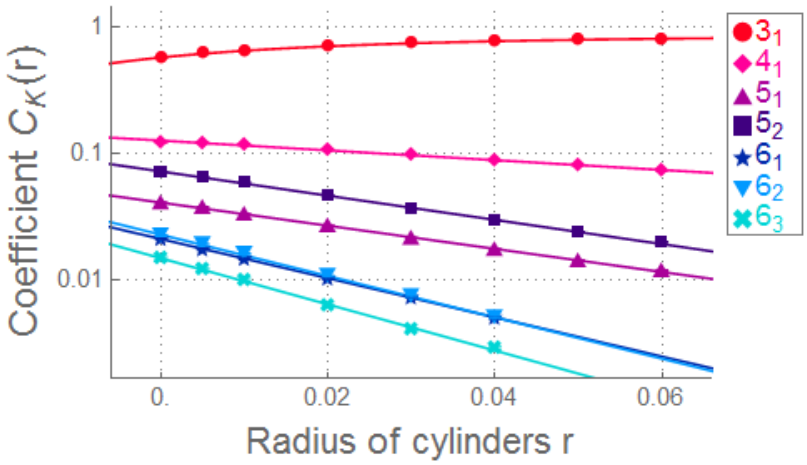

Figure 3.5. Coefficients C_K for the several prime knots are plotted against the cylindrical radius r in the logarithmic scale.

The estimated C_K for the 3_1 knot grows gradually as r grows. We found that the following formula well expresses the estimated C_K values for the 3_1 knot:

$$C_K(r) = c_0 - c_1 Exp(-d_1 r). \tag{3.10}$$

The fitting curves to the estimated C_K values for the other prime knots are given by another formula:

$$C_K(r) = c_1 Exp(-d_1 r). \tag{3.11}$$

The best estimates of c1, c0 and d1 and χ^2/DF values are shown in the following table.

	c1	c0	d1	χ 2/DF
3_1 knot	0.2753 ± 0.0021	0.8515 ± 0.0023	31.99 ± 0.63	0.76
4_1 knot	0.1259 ± 0.0012	-	8.94 ± 0.28	8.32
5_1 knot	0.04052 ± 0.00032	-	21.13 ± 0.27	1.39
5_2 knot	0.07159 ± 0.00058	-	22.12 ± 0.27	3.06
6_1 knot	0.0208 ± 0.000096	-	35.79 ± 0.23	0.2

6_2 knot	0.02252 ± 0.00019	-	37.77 ± 0.37	0.68
6_3 knot	0.01464 ± 0.00031	-	42.18 ± 0.98	2.19

The rate of exponential decreasing d_1 becomes larger as the minimal crossing number grows. Coefficient C_{31} becomes slightly larger as r grows. Thus, the ratio among coefficient C_K is approximately

$$\begin{aligned} C_{31}: C_{41}: C_{51}: C_{52} &= 14: 3: 1: 1.8, for\ r = 0 \\ C_{31}: C_{41}: C_{51}: C_{52} &= 27: 4: 1: 1.7, for\ r = 0.02 \\ C_{31}: C_{41}: C_{51}: C_{52} &= 68: 6: 1: 1.6, for\ r = 0.06 \end{aligned} \tag{3.12}$$

Since the characteristic length N_K and the exponent m(K) are constant for any prime knot, only coefficient C_K characterizes the knot probability for the prime knots and the quotient of the knot probability for a prime knot over that for another knot is given by the ratio of C_K.

$$\frac{P(N; r, K)}{P(N; r, K')} = \frac{C_K}{C_K'}, K\ is\ given\ by\ a\ prime\ knot. \tag{3.13}$$

Equation (3.13) and (3.12) predict that if we produce such ring polymers that have strong excluded volume effect, like DNA, ring polymer with the 3_1 knot dominates over ring polymers with other prime knots.

Universal curves

Since the exponent m(K) is close to 1 for the prime knots and the various values of the radius of cylinders r, the knot probabilities of the prime knots are characterized by the coefficient C_K and the characteristic length N_K. We can normalize the knot probabilities for the prime knots and the radius r and obtain the universal curves of the knot probabilities of the prime knots.

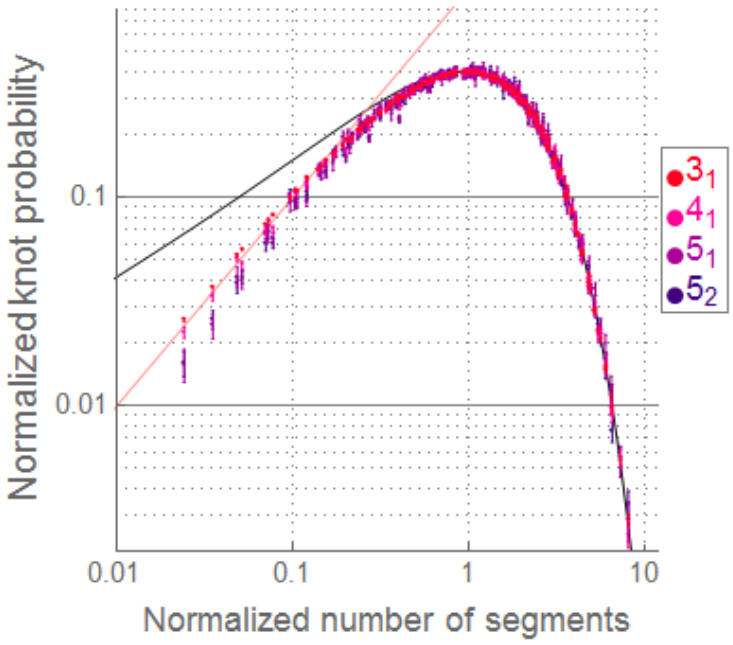

Figure 3.6 Universal curve.

In the figure, the black line is given by the normalized formula of the equation (3.8), $P_x(x) = x\Gamma(x+1)/x^{x-1/2}/\sqrt{2\pi}$, the red line is given by y=x. The universal curve is close to the normalized formula when x is larger than 0.5 and it approaches y=x when x is smaller than 0.1.

3.3 Knot probability for composite knots

The knot probabilities for several composite knots are plotted against the number of segments N in the following figures. The fitting curves are given by formula (3.8) for different values of the cylindrical radius r.

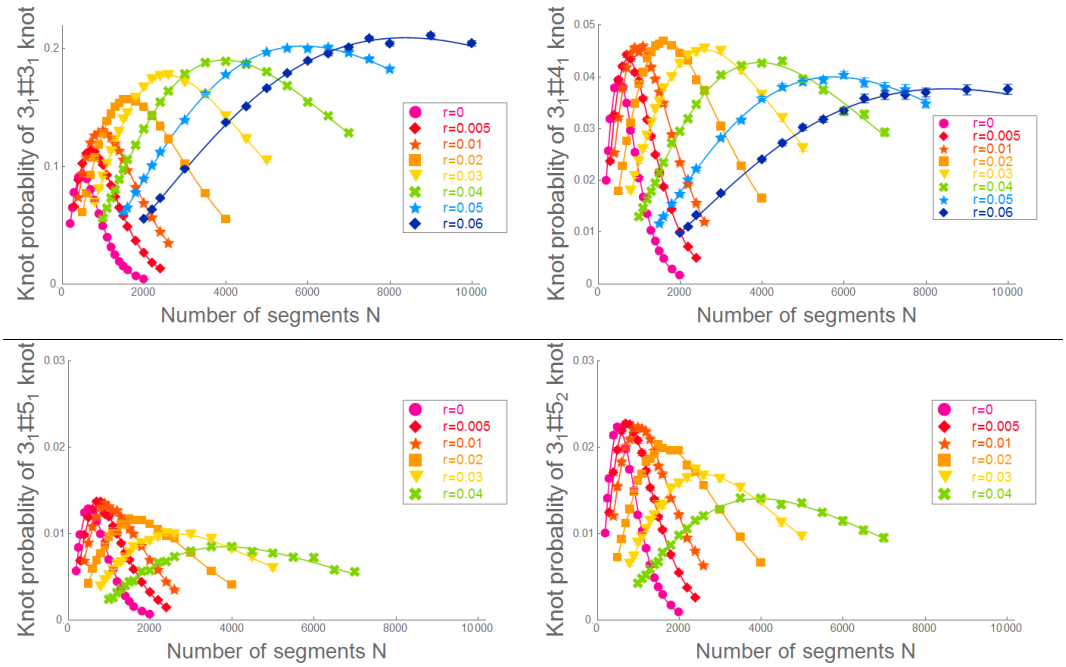

Figure 3.7 The knot probabilities for composite knots

Coefficient C_K

For on-lattice RP, parameter C_K for the knot probability of composite knot is expressed approximately as follows [42].

$$C_{K\#K'} = C_K C'_K, \text{if } K \neq K'$$
$$C_{K\#K} = \frac{C_K^2}{2!}, \tag{3.14}$$

Then we obtain the formula that expresses coefficient C_K for a given composite knot from eq. (3.10) and (3.11):

$$C_{K\#K'} = c_1 c'_1 Exp(-(d_1 + d'_1)r), \text{if } K \neq K', K, K' \neq 3_1 \; knot. \tag{3.15}$$

Now we show that eq. (3.14) can be applicable for C_K estimated from the knot probability fitted by eq. (3.7) of off-lattice SAP. Figure 3.7 shows coefficients C_K for several composite knots. The curves are the value of C_K expected from eq. (3.15) and

the points are the value of C_K estimated from fitting. They are similar each other, but there are differences larger than error bars when r=0.

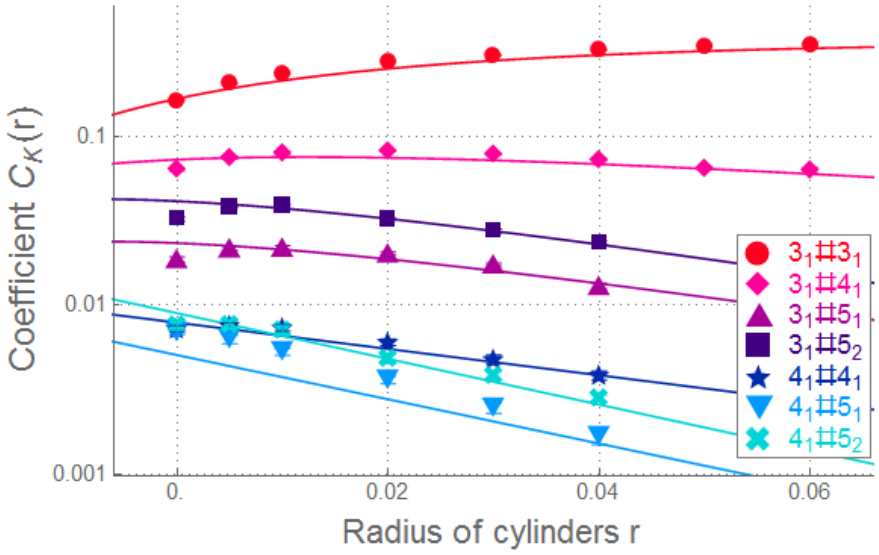

Figure 3.8 Coefficient C_K for composite knots including 2 prime knots

4 Radius of gyration

4.1 Results for MS radius of gyration of knotted polygons

In this section, we show our numerical results for the topological effects in knotted polygons. In the following figure, the mean-square (MS) radius of gyration of RP and SP without topological constraints is plotted against the number of segments N in the double-logarithmic scale. Here the notation "All knot" means the ensemble of RP or SAP without topological constraints. The fitting curves are given by $\langle R_g^2 \rangle_K = A_1 N(1 + b_1 / \sqrt{N})$.

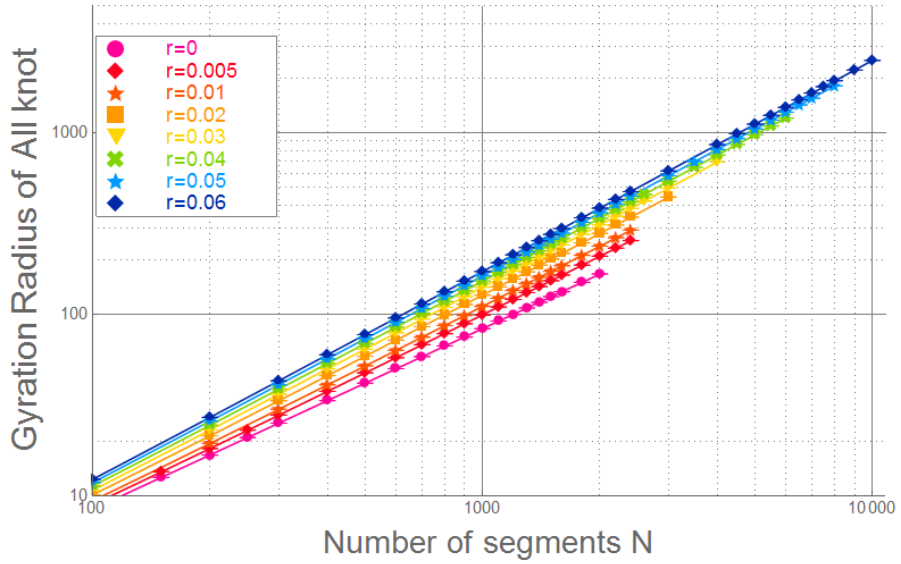

Figure 4.1 MS radius of gyration of polygons without topological constraint is plotted against the number of segments N in double logarithmic scale.

The MS radius of gyration is proportional to the power of the number of segments N. Its exponent is 0.5 for RP or 0.59 for SAP consisting of the cylinders with enough large cylindrical radius. The scaling law of the radius of gyration of RP or SAP is well-known.

Now we compare the MS radius of gyration of RP or SAP with topological constraint with that of RP or SAP without topological constraint in order to estimate the topological swelling in a knotted polymer.

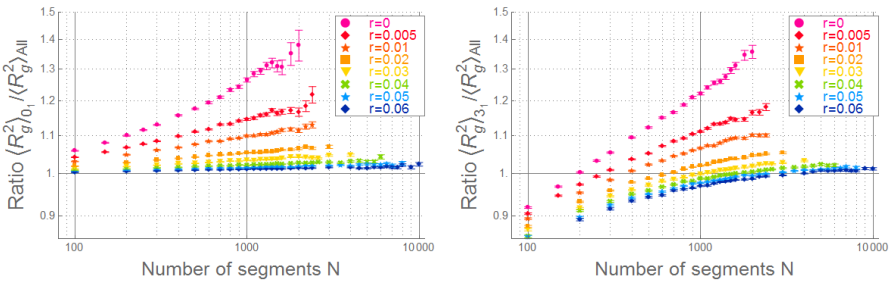

Figure 4.2 Ratio of the MS radius of gyration of knotted polygons to that of polygons without topological constraint is plotted against the number of vertices N in double logarithmic scale.

In the figure 4.2, the ratios of the MS radius of gyration of RP or SAP with given knot type K to that of RP or SAP without topological constraint are plotted against N in the double-logarithmic scale.

In case of RP, the ratio increases as N grows and seems to continue increasing. Conversely, the ratio of SAP with cylindrical radius 0.1 is nearly constant in case of the trivial knot. In case of the 3_1 knot, the ratio of SAP increases when N is small, but it seems to converge. Thus we conjectured the topological effect in MS radius of gyration of a knotted polygon raises the scaling exponent only in a Θ-solvent and it changes coefficient A_1 but does not affect the scaling exponent in a good solvent.

4.2 Results for polymers with other topologies

Polymers with various topologies have been synthesized chemically due to recent developments in experimental techniques [11, 12, 13, 14]. For instance, chemists succeeded in synthesizing double-ring polymers, tadpole-shaped polymers and caged polymers. In this section, we give brief illustration of their properties evaluated through simulation.

Double-ring polymers

We evaluated the mean square (MS) radius of gyration of double-ring polymers through off-lattice self-avoiding double polygons consisting of cylinders of unit length with radius r [36]. We numerically showed that several physical properties of double-ring polymers depend on the linking number of the constituent twin ring polymers in the double polymer.

We generated a self-avoiding double polygon which is a pair of equilateral self-avoiding polygons connected by a cylinder of unit length with radius r by Monte-Carlo method. Here the number of vertices of the polygons is n_1. Any pair of the cylinders of the self-avoiding double polygon has no overlaps. If the cylindrical radius is 0, we call such double polygon an ideal double polygon.

In fig. 4.3, the MS radius of gyrations of double polygons with or without excluding volume and that of RP and SAP versus the number of vertices are plotted in the double-logarithmic scale. The MS radius of gyration of double polygons with the number of vertices $2n_1+1$, which have two constituent $2n_1$-gons and a segment connecting them, is smaller than that of polygons with the number of vertices $2n_1$.

The ratio of the MS radius of gyration for double polygons to that for polygons is given by 0.70 for r=0 or 0.77 for r=0.1. The ratio grows and approaches 1.0 as the cylindrical radius increases. We considered the reason why the ratio increases: In an ideal double polygon, segments come near the connecting segment. Thus the total size of the ideal double polygon becomes smaller than that of the ideal polygon of almost same number of vertices. However, under the excluded volume effect, segments near the connecting segment repel each other and the total size of the self-avoiding double polygon becomes larger than that of the case without excluded volume.

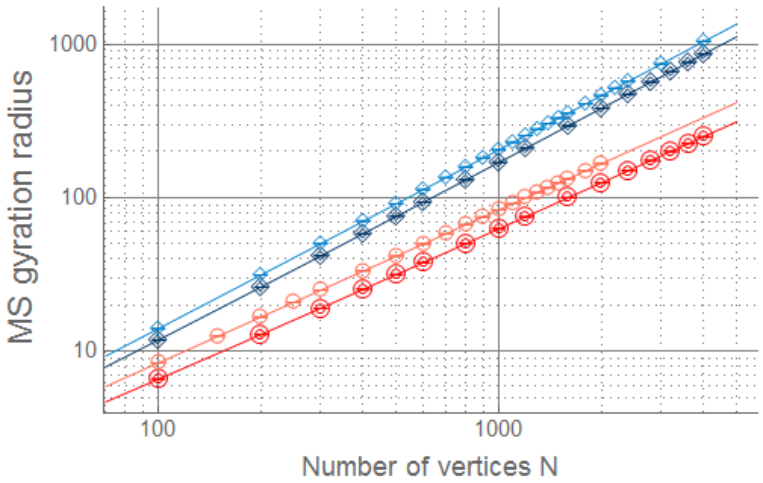

Figure 4.3 The MS radius of gyration of double polygons without topological constraint versus the number of vertices. Here the red double circles correspond to the MS radii of gyration of random double polygons, the pink circles those of random polygons, the blue double diamonds those of self-avoiding double polygons and the right-blue diamonds those of SAP.

We can define the linking number of the constituent twin polygons in a self-avoiding double polygon. Some statistical properties of self-avoiding double polygons depend on the linking number: The MS radius of gyration of the self-avoiding double polygons with linking number 0 is larger than that of the self-avoiding double polygons with non-zero linking number. Moreover, the larger linking number self-avoiding double polygons in an ensemble have, the smaller the MS radius of gyration of it as shown in the following figure. The diffusion coefficient of the self-avoiding double polygons with linking number 0 is smaller than that of of the self-avoiding double polygons with other linking numbers.

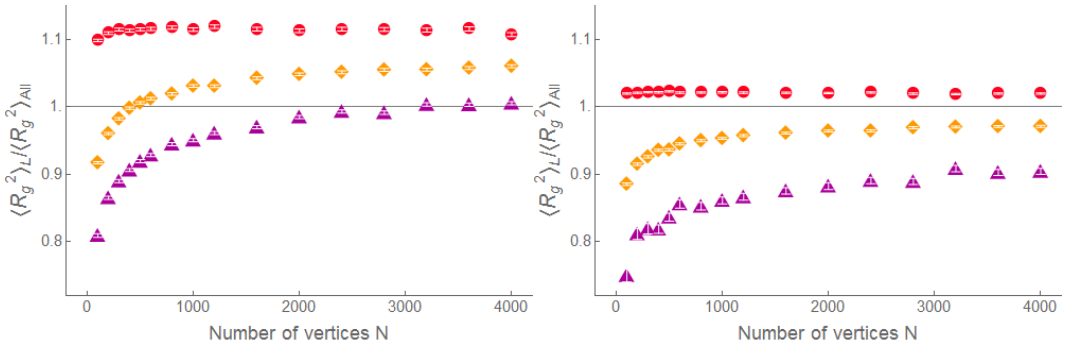

Figure 4.4 The ratio of MS radius of gyration of the linked double polygons to that of the double polygons without topological constraint is plotted against the number of vertices N. The left figure is the data of double polygons without excluding volume and the right one is those of double polygons consisting of cylinders with radius r=0.1. The red circles, yellow diamonds and purple triangles are correspond to the ratio for L=0, 1 and 2 respectively.

The probability that the constituent polygons of a self-avoiding double polygon have a linking number L is expressed by a function of n1. The linking probability for L=0 decays as a power of n1. Remark this is different from the case of a knot probability for polygons. The probability that a polygon has the topology given by the trivial knot decay exponentially as the number of vertices of the polygon grows. The linking probability for other linking numbers decreases as n1 increases while n1 is enough large, though it increases as n1 increases while n1 is small.

Caged polymers

A caged polymer is a variety of a ring polymer that has subchains of which both ends are connected each other. For example, a ring polymer has a pair of subchains that are connected at both endpoints and a theta-shaped polymer has a triplet of such subchains as shown in figure 4.5.

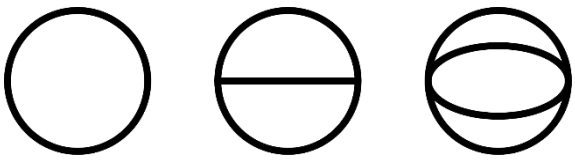

Figure 4.5 Caged polymers.

We numerically evaluated the MS radius of gyration of caged polymers for the several number of subchains f [35]. We generated a non-equilateral random polygon and non-equilateral random walks which start from a vertex of the polygon and end at the antipodal vertex of the polygon. We call it a caged polygon. Here the sum of the number of random walks and 2 corresponds to the number of subchains.

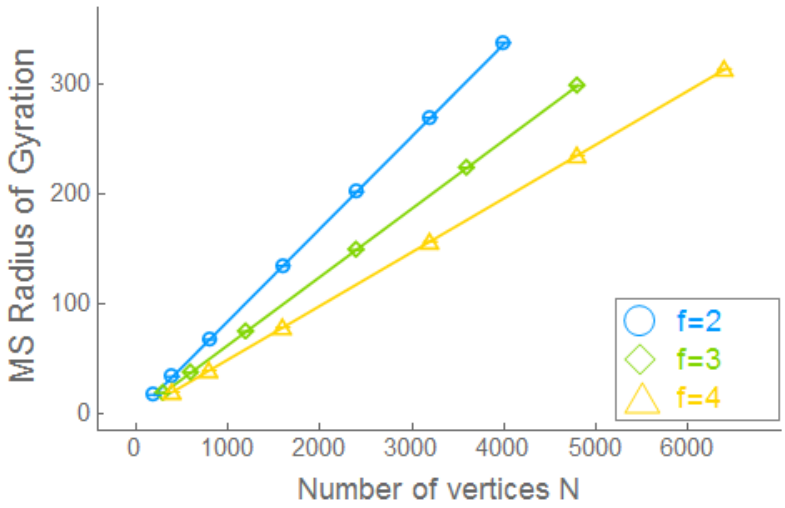

Figure 4.6 MS radius of gyration of caged polymers is plotted against the number of vertices.

In fig. 4.6 we show the MS radius of gyration of caged polygons. The fitting curves are given by $\langle R_g^2 \rangle_K = A_1 N(1 + b_1 / \sqrt{N})$. The MS radius of gyration of caged polygons with f=2 (ring) is largest and that of caged polygons with f=3 is second largest. The MS radius of gyration of caged polygons becomes smaller as f increases.

Appendix 1 Polymer statistics and Critical Phenomena

In this section, we show the relationship between polymer statistics and critical phenomena which is raised in a system approaching the second order phase transition points. Critical phenomena includes the power-law divergences of several physical quantities: the correlation length, the specific heat, and the magnetic susceptibility. These quantities can be represented by the power of T_c-T, where T_c is the critical temperature. We call the exponent of the divergence the critical exponent. We show that the divergence of physical quantities in critical phenomena corresponds to the scaling nature in the polymer statistics [6].

Critical exponents in magnetic phase transition

We consider the magnetic atoms on a lattice. Each atom has a spin S_i which is a vector with n components. We introduce critical exponents ν, α, β, γ. The critical exponents does not depend on the microstructure of the lattice nor the detail of interactions but the dimension d and the number of components n.

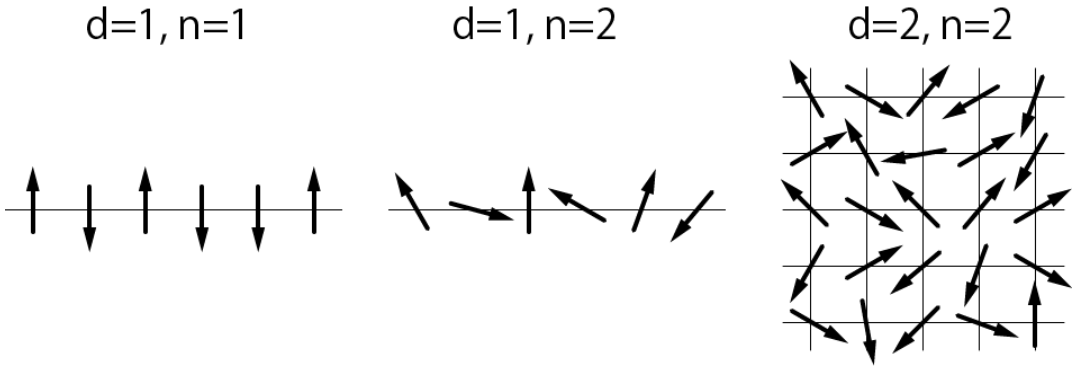

Figure 1.1 Dimension d and the number of components n

Replace the gap of the temperature of the system from the critical temperature by ϵ :

$$\epsilon = \frac{T - T_c}{T_c} \tag{A1.1}$$

Although the average magnetization is zero, there are small domains where spins are correlated in disordered phase. The characteristic length of these domains is correlation length ξ . ξ diverges as the system approaches the critical temperature.

$$\xi \sim |\epsilon|^{-\nu} \tag{A1.2}$$

Critical exponent ν corresponds to the scaling exponents of polymer chains. Here $\epsilon^{-1} \sim N$.

Specific heat diverges in the form

$$\mathrm{C} = C_0 |\epsilon|^{-\alpha}. \tag{A1.3}$$

without external magnetic field, magnetization is

$$\mathrm{M} = M_0 |\epsilon|^{\beta} \tag{A1.4}$$

Magnetic susceptibility is

$$\chi_{\mathrm{M}} = \chi_0 |\epsilon|^{-\gamma} \tag{A1.5}$$

In the next section, we focus on the n-vector model of the spin system. The expanded partition function of the n-vector model corresponds to closed SAW.

Partition function of the n-vector model

The norm of S_i is fixed and we choose the following normalization:

$$\mathbf{S_i^2} = \sum_{\alpha=1}^{n} S_{i\alpha}^2 = n. \tag{A1.6}$$

We ignore all quantum effects. Define the model through the following Hamiltonian:

$$\mathcal{H} = -\sum_{\mathrm{i>j}} K_{ij} \boldsymbol{S_i} \boldsymbol{S_j}, \tag{A1.7}$$

where Kij is positive if i and j are neighboring sites and zero if not. Here we choose the external magnetic field is zero. The number of neighboring sites depends on the lattice. For example, one site has 4 neighboring sites on the 2-dimensional cubic lattice.

The partition function is the product over all pairs of i and j

$$\mathrm{Z} = \prod_{i>j}^{N} \int d\Omega_i Exp\left(-\frac{\mathcal{H}}{\tau}\right), \tag{A1.8}$$

where dΩ is the integration over all available orientations of a spin. Ω is the total

volume of the integration as follows:

$$\mathrm{d}\Omega = \prod_{l}^{n-1} r(sin\theta_l)^{n-l-1}.$$
$$\Omega = \prod_{i} \int d\Omega_i \tag{A1.9}$$

We expand the partition function in power series of couples of spins by an approximation e^(-x)=1-x+x^2-⋯

$$Exp\left(-K_{ij}\,(\boldsymbol{S_i S_j})/\tau\right)$$
$$= 1 - \frac{K_{ij}}{\tau}(\boldsymbol{S_i S_j}) + \frac{1}{2!}\left(\frac{K_{ij}}{\tau}\right)^2 (\boldsymbol{S_i S_j})^2 - \cdots \tag{A1.10}$$

Substituting (A1.10) to (A1.7) and multiplying over the pairs of i and j, we obtain a complex formula. However, it becomes simple when we take the limit n→0 since this procedure removes terms of which degree is larger than 2. We can formally solve the partition function in this limit although n is a natural number by definition. The result corresponds to all of the closed SAWs.

Moment theorem

In this section, we introduce the moment theorem to reduce the partition function in the limit n→0. We have following terms in the expanded partition function:

$$\langle S_{i\alpha}\rangle_0, \langle S_{i\alpha}S_{i\beta}\rangle_0, \langle S_{i\alpha}S_{i\beta}S_{i\gamma}\rangle_0, \ldots, \tag{A1.11}$$

where α, β, and γ are component subscripts, $\langle\ \rangle_0$ means an average over the allowed orientations of all spins and $\langle\ \rangle_T$ means an thermal average.

$$\langle A\rangle_0 = \prod_{i>j}^{N} \int A d\Omega_i.$$
$$\langle A\rangle_T = \frac{\langle Exp(-\mathcal{H}/\tau)A\rangle_0}{\langle Exp(-\mathcal{H}/\tau)\rangle_0}. \tag{A1.12}$$

The moment theorem show us that only quadratic averages of spins does not vanish in the limit n→0.

The first-order moment of a spin component is zero because spins satisfy rotational symmetry:

$$\langle S_{i\alpha} \rangle_0 = 0. \tag{A1.13}$$

By the equation (A1.13), the second-order moment of a spin is 1 if $\alpha = \beta$, 0 if not.

$$\langle S_{i\alpha} S_{i\beta} \rangle_0 = \delta_{\alpha\beta}. \tag{A1.14}$$

For higher moments, the characteristic function derives that they are zero when n=0 (see appendix).

Partition function expanded in self-avoiding loops

Now we expand the partition function of the n-vector model and show that the result is expressed in self-avoiding loops.

According to the moment theorem, only second-order moments of spins survive. Therefore the partition function is expanded in the following form:

$$\begin{aligned} &\frac{Z}{\Omega} \\ &= \langle \prod_{i>j} Exp\left(\frac{K_{ij}}{\tau} \sum_{\alpha} S_{i\alpha} S_{j\alpha} \right) \rangle_0 \\ &= \langle \prod_{i>j} \left\{ 1 + \frac{K_{ij}}{\tau} \sum_{\alpha} S_{i\alpha} S_{j\alpha} + \frac{1}{2} \left(\frac{K_{ij}}{\tau} \right)^2 \sum_{\alpha} \sum_{\beta} S_{i\alpha} S_{j\alpha} S_{i\beta} S_{j\beta} \right\} \rangle_0. \end{aligned} \tag{A1.15}$$

An average $\langle\ \rangle_0$ is equal to a thermal average of which energy is zero, namely, the spins do not have correlations. Since the spins are independent each other,

$$\langle S_{i\alpha} S_{j\alpha} \rangle_0 = \langle S_{i\alpha} \rangle_0 \langle S_{j\alpha} \rangle_0 \tag{A1.16}$$

Using the equation (A1.16), we remove the terms in which $\alpha \neq \beta$.

$$\begin{aligned} &\langle \sum_{\alpha} \sum_{\beta} S_{i\alpha} S_{j\alpha} S_{i\beta} S_{j\beta} \rangle_0 \\ &= \sum_{\alpha} \langle S_{i\alpha} S_{j\alpha} S_{i\alpha} S_{j\alpha} \rangle_0 \\ &= \sum_{\alpha} \langle S_{i\alpha} S_{i\alpha} \rangle_0 \langle S_{j\alpha} S_{j\alpha} \rangle_0. \end{aligned} \tag{A1.17}$$

If i is equal to j at the second line in (A1.17), the third line becomes the forth-order

moment of spins and it is zero.

We illustrate term $K_{ij}^2\langle S_{i\alpha}S_{j\alpha}S_{i\alpha}S_{j\alpha}\rangle_0$ by the loop between neighboring sites as follows:

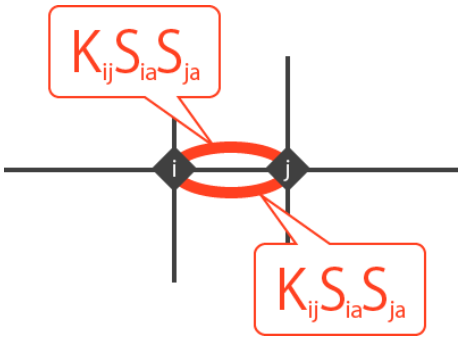

Figure 1.2 Illustrated $K_{ij}^2\langle S_{i\alpha}S_{j\alpha}S_{i\alpha}S_{j\alpha}\rangle_0$

Figure 1.2 where the lines connecting i and j express $\mathrm{K_{ij}}\langle S_{ia}S_{ja}\rangle_0$. $K_{ij}^2\langle S_{i\alpha}S_{i\alpha}S_{j\alpha}S_{j\alpha}\rangle_0$ corresponds to the pair of lines which connect neighboring sites i and j because $\mathrm{K_{ij}}$ is zero if i and j are not nearest neighboring.

The terms of the expanded partition function are represented by closed lines. The moment theorem requires that each spin makes a pair with a spin on the identical atom, namely, each site has two line segments. In addition, $\mathrm{K_{ij}}$ requires that i and j are neighboring, which means that the line segments are continuous and connect a pair of neighboring sites. Hence all the self-avoiding loops represent the surviving terms in the expanded partition function.

For another example, we consider an eighth-order term $K_{ij}K_{jk}K_{kl}K_{li}\langle S_{i\alpha}S_{j\alpha}S_{j\alpha}S_{k\alpha}S_{k\alpha}S_{l\alpha}S_{l\alpha}S_{i\alpha}\rangle_0$. We illustrate such terms that {i, j, k, l} = {1, 2, 10, 9} and {18, 19, 26, 27} in the following figure by regular rectangles.

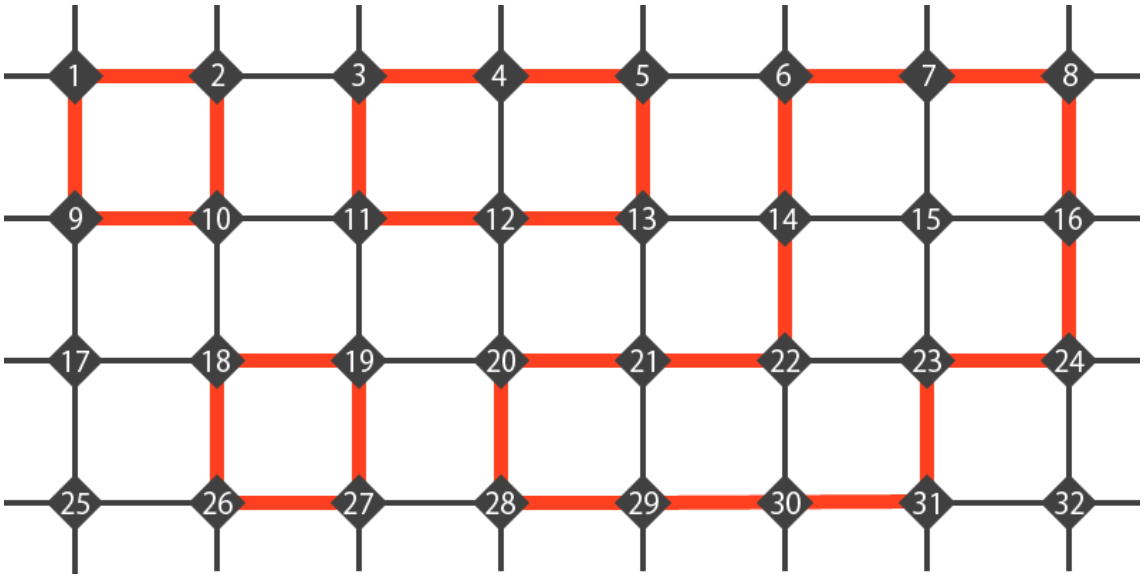

Figure 1.3 Some illustrated terms

Correlation and self-avoiding walks between two sites

In this section, we explain that the correlation between two sites, i and j, is associated with all SAW which connect i and j sites.

The correlation between two spins is defined by:

$$\langle S_{ia} S_{ja} \rangle = \frac{\langle Exp\left(-\frac{\mathcal{H}}{\tau}\right) S_{ia} S_{ja} \rangle_0}{\langle Exp\left(-\frac{\mathcal{H}}{\tau}\right) \rangle_0}. \qquad \text{(A1.18)}$$

The denominator at the right-hand side is 1.

Expanding (A1.18), we obtain

$$
\begin{aligned}
&\langle S_{ia}S_{ja}\rangle \\
&= \langle S_{ia}S_{ja}\prod_{k>l} Exp\left(\frac{K_{kl}}{\tau}\sum_{\alpha} S_{k\alpha}S_{l\alpha}\right)\rangle_0 \\
&= \langle S_{ia}S_{ja}\prod_{k>l}\left\{1-\frac{K_{kl}}{\tau}\sum_{\alpha} S_{k\alpha}S_{l\alpha}+\frac{1}{2}\left(\frac{K_{kl}}{\tau}\right)^2\sum_{\alpha} S_{k\alpha}S_{l\alpha}S_{k\alpha}S_{l\alpha}\right\}\rangle_0 \qquad \text{(A1.19)} \\
&= \langle S_{ia}S_{ja}\prod_{i>j}\left\{1-\frac{K_{kl}}{\tau}\,S_{ka}S_{la}+\frac{1}{2}\left(\frac{K_{kl}}{\tau}\right)^2\,S_{ka}S_{la}S_{ka}S_{la}\right\}\rangle_0 \\
&= \langle S_{ia}S_{ja}\frac{K_{ij}}{\tau}\,S_{ia}S_{ja}+\cdots\rangle_0.
\end{aligned}
$$

The spin correlation corresponds to all sequence of continuous lines, which connect i and j. All terms in the expanded correlation have a coefficient (K/ τ)^N. Thus

$$\langle S_{ia}S_{ja}\rangle = \sum_{N}\Re_N(i,j)\left(\frac{K}{\tau}\right)^N. \qquad \text{(A1.20)}$$

where $\Re_N(i,j)$ is the total number of N-step SAW connecting i and j.

Magnetic susceptibility and SAW

The number of N-step SAW is

$$\Re_N = \sum_{j}\Re_N(i,j). \qquad \text{(A1.21)}$$

We can use any integer for i because of the translational symmetry of the lattice: there are only one independent index j-i. The number $\Re_N$ is asymptotically

$$\Re_N \cong \bar{z}^N N^{\gamma-1}. \qquad \text{(A1.22)}$$

We explain the correspondence of γ in the asymptotical representation of the number of SAW to γ for the critical exponent of the magnetic susceptibility.

$$\chi_M = \frac{1}{\tau}\sum_{j}\langle S_{ia}S_{ja}\rangle. \qquad \text{(A1.23)}$$

The equation (A1.23) is the discrete expression of the definition of the magnetic susceptibility. Substituting the equation (A1.23) to the equation (A1.20), we obtain

$$\chi_M = \frac{1}{\tau}\sum_N \Re_N \left(\frac{K}{\tau}\right)^N \cong \frac{1}{\tau}\sum_N \left(\frac{K\bar{z}}{\tau}\right)^N N^{\gamma-1} \ . \tag{A1.24}$$

When $\tau = \tau_c = K\bar{z}$, the equation (A1.24) diverges. If τ is a little larger than τ_c, $\tau = \tau_c(1+\epsilon) \cong \tau_c Exp(\epsilon)$.

$$\begin{aligned} &\cong \frac{1}{\tau_c}\sum_N Exp(-\epsilon N) N^{\gamma-1} \\ &\cong \frac{1}{\tau_c}\int_0^\infty dN\, Exp[-\epsilon N] N^{\gamma-1} \\ &= \frac{1}{\tau_c}\int_0^\infty dN \frac{1}{\epsilon} Exp[-t] \left(\frac{t}{\epsilon}\right)^{\gamma-1} \\ &= \frac{\epsilon^{-\gamma}}{\tau_c}\Gamma(\gamma) \\ &\propto \epsilon^{-\gamma}. \end{aligned} \tag{A1.25}$$

Appendix 2 Moment theorem

In this appendix, we review the moment theorem which explain that all averages of spins are 0 except the quadratic average of spins.

Definition of the characteristic function

Define the characteristic function for the variable X as follows.

$$f(k) = E\left[e^{ikX}\right] = \int_{-\infty}^{\infty} e^{ikx} p_X(x) dx. \tag{A2.1}$$

where $p_X(x)$ is the probability density function (PDF) of X. Since the characteristic function is the inverse Fourier transform of PDF, it has all information of PDF.

The derivative of the characteristic function is

$$\begin{aligned} &\frac{d}{dk} f(k) \\ &= \int_{-\infty}^{\infty} \frac{d}{dk} e^{ikx} p_X(x) dx \\ &= -i \int_{-\infty}^{\infty} x e^{ikx} p_X(x) dx \,. \end{aligned} \tag{A2.2}$$

Substitute 0 to k,

$$\begin{aligned} &\to -i \int_{-\infty}^{\infty} x p_X(x) dx \\ &= -iE[X]. \end{aligned} \tag{A2.3}$$

The n-th order derivative of the characteristic function is

$$\frac{d^n}{dk^n} f(k)|_{k=0} = (-i)^n E[X^n]. \tag{A2.4}$$

The n-th order derivative of the characteristic function provides the n-th order center moment of X.

Average of spins

The characteristic function of spins is defined by

$$f_i(\boldsymbol{k}) = \langle Exp(i\boldsymbol{k} \cdot \boldsymbol{S_i}) \rangle_0. \tag{A2.5}$$

Here, PDF of spins is expressed as follows.

$$p(x)dx = \prod_{l=1}^{n-1} \left\{ \left(sin\theta_j \right)^{n-l-1} r d\theta_l \right\} \Big/ \Omega. \tag{A2.6}$$

We can express the average of spins by the characteristic function of spins. For instance, the quadratic average of spins is

$$\langle S_{i\alpha} S_{i\beta} \rangle_0 = (-i)^2 \frac{\partial}{\partial k_\alpha} \frac{\partial}{\partial k_\beta} f_i(\boldsymbol{k})|_{\boldsymbol{k}=0}. \tag{A2.7}$$

We try to represent the characteristic function of spins as an analytic form.

The Laplacian of the characteristic function of spins is

$$\begin{aligned}
&\nabla^2 f_i(\boldsymbol{k}) \\
&= \sum_\alpha \frac{\partial^2}{\partial k_\alpha^2} f_i(\boldsymbol{k}) \\
&= \sum_\alpha \int \frac{\partial^2}{\partial k_\alpha^2} Exp(i\boldsymbol{k} \cdot \boldsymbol{S_i}) d\Omega / \Omega \\
&= \sum_\alpha \int -S_{i\alpha}^2 Exp(i\boldsymbol{k} \cdot \boldsymbol{S_i}) d\Omega / \Omega \\
&= -\sum_\alpha \langle S_{i\alpha}^2 Exp(i\boldsymbol{k} \cdot \boldsymbol{S_i}) \rangle_0 \\
&= -\langle \sum_\alpha S_{i\alpha}^2 Exp(i\boldsymbol{k} \cdot \boldsymbol{S_i}) \rangle_0 \\
&= -\langle n Exp(i\boldsymbol{k} \cdot \boldsymbol{S_i}) \rangle_0 \\
&= -n f_i(\boldsymbol{k}).
\end{aligned} \tag{A2.8}$$

The characteristic function of spins depends on the only norm of k. We can rewrite the derivatives of characteristic function as the function of the norm of k. The 1st order derivative is expressed as follows.

$$\frac{\partial}{\partial k_\alpha} f = \frac{\partial k}{\partial k_\alpha} \frac{\partial f}{\partial k} = \frac{k_\alpha}{k} \frac{\partial f}{\partial k}. \tag{A2.9}$$

The 2nd order derivative is

$$
\begin{aligned}
&\frac{\partial^2}{\partial k_\alpha^2} f \\
&= \left(\frac{\partial}{\partial k_\alpha}\frac{k_\alpha}{k}\right)\cdot\left(\frac{\partial f}{\partial k}\right) + \frac{k_\alpha}{k}\frac{\partial}{\partial k_\alpha}\left(\frac{\partial f}{\partial k}\right) \\
&= \frac{1}{k}\left(\frac{\partial f}{\partial k}\right) + \frac{k_\alpha}{k}\frac{\partial}{\partial k}\frac{\partial k}{\partial k_\alpha}\left(\frac{\partial f}{\partial k}\right) \\
&= \frac{1}{k}\left(\frac{\partial f}{\partial k}\right) + \frac{k_\alpha^2}{k}\frac{\partial}{\partial k}\left(\frac{1}{k}\frac{\partial f}{\partial k}\right).
\end{aligned}
\tag{A2.10}
$$

Hence we rewrite the Laplacian of the characteristic function of spins:

$$
\begin{aligned}
&\nabla^2 f \\
&= \sum_\alpha \left(\frac{1}{k}\frac{\partial f}{\partial k} + \frac{k_\alpha^2}{k}\frac{\partial}{\partial k}\left(\frac{1}{k}\frac{\partial f}{\partial k}\right)\right) \\
&= \frac{n}{k}\frac{\partial f}{\partial k} + k\frac{\partial}{\partial k}\left(\frac{1}{k}\frac{\partial f}{\partial k}\right) \\
&= \frac{n-1}{k}\frac{\partial f}{\partial k} + \frac{\partial^2 f}{\partial k^2}.
\end{aligned}
\tag{A2.11}
$$

Compare (A2.8) with (A2.11),

$$
\frac{\partial^2 f}{\partial k^2} + \frac{n-1}{k}\frac{\partial f}{\partial k} + nf = 0. \tag{A2.12}
$$

By the equation (A2.5), there are 3 boundary conditions as follows.

$$
\begin{aligned}
f(0) &= 1, \\
\frac{\partial}{\partial k} f|_{k=0} &= 0, \\
\frac{\partial^2}{\partial k^2} f|_{k=0} &= -1.
\end{aligned}
\tag{A2.13}
$$

Substitute the boundary conditions to the differential equation (A2.12),

$$
\frac{\partial^2 f}{\partial k^2} - \frac{1}{k}\frac{\partial f}{\partial k} = 0. \tag{A2.14}
$$

Therefore

$$
f = \pm\frac{1}{2}Ck^2 + C_0. \tag{A2.15}
$$

The values of C and C_0 which satisfy the boundary conditions are $\pm C = -1, C_0 = 1$. We get the characteristic function of spins.

$$f = 1 - \frac{1}{2}k^2. \tag{A2.16}$$

Since the 3rd or higher degree derivative of the equation (A2.16) is 0, the higher averages of spins are 0.

References

1 A. Takano et al, Macromolecules **45**, 369-373 (2012)

2 M. A. Krasnow, A. Stasiak, S. J. Spengler, F. Dean, T. Koller and N. R. Cozzarelli, Nature **304**, 559 (1983).

3 V. V. Rybenkov et al, PNAS **90**, 5307-5311 (1933)

4 S.Y. Shaw and J.C. Wang, Science **260**, 533 (1993).

5 N. Madras and G. Slade, *The Self-Avoiding Walk*, (Birkhaeuser, Boston, 1993)

6 P. G. de Gennes, *Scaling Concepts in Polymer Physics*, (Cornell Univ. Press, Ithaca and New York, 1979)

7 M. Polyak and O. Viro, IMRN **11**, 445 (1994)

8 M. D. Frank-Kamenetskii and A. V. Vologodskii, Sov. Phys. Usp. Fiz. Nauk 134, 641-673 (1981)

9 H. L. Frisch and E. Wasserman, J. Amer. Chem. Soc., **83**, 3789 (1961)

10 M. Delbrück, in *Mathematical Problems in the Biological Sciences*, ed. by R. E. Bellman, Proc. Symp. Appl. Math., **14**, 55 (1962)

11 H. Oike, H. Imaizumi, T. Mouri, Y. Yoshioka, A. Uchibori, and Y. Tezuka, J. Am. Chem. Soc. **122**, 9592 (2000).

12 A. Takano, Y. Kushida, K. Aoki, K. Matsuoka, K. Hayashida, D. Cho, D. Kawaguchi and Y. Matsushita, Macromolecules **40**, 679(2007

13 B. A. Laurent and S. Grayson, J. Am. Chem. Soc. **128**, 4238{4239 (2006).

14 *Topological Polymer Chemistry: Progress in cyclic polymers in syntheses, properties and functions*, ed. by Y. Tezuka, (World Scientic Publ., Singapore, 2013).

15 D.W. Sumners and S. Whittington J. Phys. A: Math. Gen., **21**, 1689 (1988).

16 N. Pippenger, Discrete Appl. Math., **25**, 273 (1989).

17 A.V. Vologodskii, A.V. Lukashin, M.D. Frank-Kamenetskii, and V.V. Anshelevich, Sov. Phys. JETP, **39**, 1059 (1974).

18 J. P. J. Michels and F. W. Wiegel, Phys. Lett. **90A**, 381 (1982).

19 T. Deguchi and K. Tsurusaki, Phys. Lett. A **174** (1993) 29-37.

20 T. Deguchi and K. Tsurusaki, J. Phys. Soc. Jpn. **62**, 1411 (1993).

21 T. Deguchi and K. Tsurusaki, J. Knot Theory Ramif. **3**, 321 (1994).

22 T. Deguchi and K. Tsurusaki, Phys. Rev. E. **55**, 6245 (1997).

23 T. Deguchi and K. Tsurusaki, in *Lectures at Knots '96*, ed. S. Suzuki, (World Scientic, Singapore, 1997) p. 95.

24 E. Orlandini, M.C. Tesi, E.J. Janse van Rensburg, and S.G. Whittington, J. Phys. A: Math. Gen., **29**, L299 (1996).

25 E. Orlandini, M.C. Tesi, E.J. Janse van Rensburg, and S.G. Whittington, J. Phys. A: Math. Gen., **31**, 5953 (1998).

26 M. Baiesi, E. Orlandini and A.L. Stella, The entropic cost to tie a knot, J. Stat. Mech., P06012(2010).

27 A. Yao, H. Matsuda, H. Tsukahara, M. K. Shimamura, and T. Deguchi, J. Phys. A: Math. Gen., **34**, 7563 (2001).

28 M. K. Shimamura and T. Deguchi, Phys. Lett. A **274**, 184-191 (2000)

29 M. K. Shimamura and T. Deguchi, J. Phys. Soc. Jpn. **70**, No. 6 1523-1536 (2001)

30 D. Rolfsen, *Knots and Links* (Publish or Perish, Wilmington DE, 1976).

31 A. Yu Grosberg and A. R. Khokhlov, *Statistical Physics of Macromolecules* (AIP press, 1994, New York).

32 J. M. Deutsch, Phys. Rev. E, **59**, R2539 (1999).

33 J. des Cloizeaux, J. Phys. Let. (France), **42** , L433 (1981).

34 A. Yu. Grosberg, Phys. Rev. Lett., **85**, 3858 (2000).

35 E. Uehara, R. Tanaka, M. Inoue, F. Hirose and T. Deguchi, Reactive and Functional Polymers **80** (2014) 48-56.

36 E. Uehara and T. Deguchi, J. Chem. Phys. **140**, 044902 (2014).

37 M. K. Shimamura and T. Deguchi, J. Phys. A: Math. Gen., **35**, L241 (2002).

38 A. Dobay, J. Dubochet, K. Millett, P. E. Sottas and A. Stasiak, Proc. Natl. Acad. Sci. USA, **100**, 5611 (2003).

39 H. Matsuda, A. Yao, H. Tsukahara, T. Deguchi, K. Furuta and T. Inami, Phys. Rev. E, **68**, 011102 (2003).

40 N. T. Moore, R. C. Lua and A. Y. Grosberg, Proc. Natl. Acad. Sci. USA, **101**, 13431 (2004).

41 D. Stigter, Biopolymers **16**, 1435 (1977).

42 A. L. Stella’s talk in “Knots and soft-matter physics”, YITP, Kyoto Univ. Aug. 26-29, 2008